Received: 8 May 2024 | Revised: 22 August 2024 | Accepted: 20 September 2024

DOI: 10.1111/sapm.12769

ORIGINAL ARTICLE

STUDIES IN APPLIED MATHEMATICS WILEY

The hysteretic Aw–Rascle–Zhang model

Andrea Corli[1] | **Haitao Fan**[2]

[1]Department of Mathematics and Computer Science, University of Ferrara, Ferrara, Italy

[2]Department of Mathematics, Georgetown University, Washington, District of Columbia, USA

Correspondence
Andrea Corli, Department of Mathematics and Computer Science, University of Ferrara, 44121 Ferrara, Italy.
Email: crl@unife.it

Funding information
European Union - Next Generation EU, PRIN 2022, Grant/Award Number: D53D23005620006; Istituto Nazionale di Alta Matematica, Grant/Award Number: CUP E53C23001670001; Gruppo Nazionale per l'Analisi Matematica, la Probabilità e le loro Applicazioni

Abstract

A novel hyperbolic system of partial differential equations is introduced to model traffic flows. This system comprises three equations, with two being linearly degenerate; its main feature is the inclusion of a hysteretic term in a generalized Aw–Rascle–Zhang (ARZ) model. First, a maximum principle for the diffusive version of the model is proven. Then, it is demonstrated that a solution to the Riemann problem exists, which is unique among solutions that are monotone in velocity; all waves exploited in the construction have suitable viscous profiles. Through several examples it is shown how, as a consequence of different driving habits, the system can model the decay, emergence, or persistence of stop-and-go waves (a feature that is missing in the ARZ model), and such behavior is characterized by a simple geometric condition. Furthermore, the model allows the study of traffic flows with a mixture of drivers whose hysteresis loops are either clockwise or counterclockwise. In particular, the presence of sufficiently many of the former dampens speed oscillations.

KEYWORDS
Aw–Rascle–Zhang model, hysteresis, Riemann solution, stop-and-go waves, string stability, traffic flows

1 | INTRODUCTION

The simplest and best known mathematical model for traffic flows is certainly the Lighthill–Whitham–Richards (LWR for short) model.[1,2] It concerns one-way flows on a straight road and can be written as

$$\rho_t + (\rho v(\rho))_x = 0, \tag{1}$$

where ρ is the vehicle concentration (or density) and v is the velocity, which is modeled as a function only depending on ρ. Usually, one assumes that v is strictly decreasing and the flux $\rho v(\rho)$ is strictly concave. However, the LWR has some inconveniences: it cannot model light traffic flows with few slow drivers[3] (in case of few drivers it prescribes that their speed must be the maximum allowed); it cannot reproduce stop-and-go waves.[4] One of the first attempts to add a second equation to the LWR model, inspired by the equation of conservation of momentum in fluid dynamics, was made by Payne and Whitham[5,6] and led to the PW model; unfortunately, also that model had serious deficiencies.

To overcome the drawbacks of LWR and PW models, Aw and Rascle[3] and, independently, Zhang,[4] proposed the system (ARZ for short)

$$\begin{cases} \rho_t + (\rho v)_x = 0, \\ (v + p(\rho))_t + v(v + p(\rho))_x = 0, \end{cases} \tag{2}$$

where p is an anticipation term with the physical dimension of a velocity; usually one assumes $p(\rho) = v^\gamma$ for $\gamma > 0$. Waves in the ARZ model always have velocity less or equal to v, a fundamental anisotropy property of traffic flows that was missing in the PW model. The ARZ model also solves some of the aforementioned inconveniences in the LWR model. First, it allows the propagation of dense car platoons with speed v in light traffic, while the LWR model let the platoon diffuse, see Section 3.1 in Ref. 4, differently of what was observed experimentally. Moreover, the ARZ model allows drivers to have different driving styles, meaning that each driver can use a speed-spacing relation different from that used by other drivers. This is manifested, in the ARZ model, by the fact that a platoon traveling steadily at the uniform speed v_0 can have varying spacing $u(x,t) = u(x)$ that propagates with each car at velocity v. On the other hand, the ARZ model still fails to model stop-and-go waves. Several papers dealt with system (2) and we can just quote few of them; Ref. 3 for the Riemann problem, Ref. 7 for a coupling of LWR and ARZ models inspired by Refs. 8, 9 for locally constrained flows, Refs. 10, 11 for networks, Ref. 12 for global existence of solutions with vacuum and BV initial data,[13–15] and for some extensions, see also Ref. 16. More general information is contained in Refs. 17, 18.

Stop-and-go waves have been interpreted in traffic flow modeling as due to a hysteretic behavior.[19–30] The reason is that the density–speed relation for *acceleration* usually differs from the same relation for *deceleration*;[28,29,31–33] the presence in the fundamental diagram of these two curves, which are connected by transverse *scanning curves*, allows for loops as in usual ferromagnetic hysteresis. However, hysteresis was never *built-in* in the previous traffic flow models. The paper[34] is the first attempt in this direction, where we added to the LWR model a second equation involving a hysteresis variable h. Such a model, called here HLWR for short, can indeed produce stop-and-go waves, which are associated with hysteretic loops. Moreover, the HLWR model can explain some issues pointed out in Refs. 35 and [4, Section 3.1], namely, that waves with speed "slightly less" than v were observed in real traffic flow, but not in LWR and ARZ model. The

HLWR can exhibit such waves because the slope of the scanning curves can be almost zero. We refer to Ref. 36 for recent advances about this topic. A microscopic version of the HLWR model is given in Ref. 37.

The aim of this paper is to introduce a hysteresis behavior into the ARZ model by including a hysteretic state variable; the corresponding model, called here HARZ, is introduced in Section 3 in Lagrange coordinates. In Section 4, we rewrite it in Euler coordinates. For completeness, the ARZ model is very briefly reviewed in Section 2, again in Lagrange coordinates. The HARZ model allows, as the HLWR model, waves propagating with speed v. However, it also allows the study of the effects of mixing drivers with different driving preferences on the triggering, growth, and decay of stop-and-go waves; this is not possible in the framework of the HLWR model. The paper[23] discovered the coexistence of both clockwise (positive) and counterclockwise (negative) hysteresis drivers in a vehicle platoon. We show that the HARZ model can model this behavior.

In Section 5, we prove a maximum principle of the viscous HARZ model, where we add a diffusive term to the equation of mass conservation. The waves used to solve the Riemann problem are introduced in Section 6; in particular, all of them have viscous profiles. Then, the existence and uniqueness of solutions to the Riemann problem is proved in Section 7; in particular, the uniqueness refers to the monotonicity property in v of the Riemann solver.

Section 8 focuses on several examples, which concretely show the effects of the heterogeneity of drivers on the decay, emergence, and persistence of stop-and-go waves; numerical simulations are also provided. We emphasize that by *decay* of a stop-and-go wave we mean the *upstream* decay of the speed oscillations in the wave, that is, as $x \to -\infty$ in Lagrange coordinates, for fixed t; such a decay is then related to the string stability.[37] We see that the decay or the persistence of a stop-and-go wave is characterized by a simple geometric condition, referred as *chord-above-scanning* condition, which is strictly related to the usual entropic chord condition in scalar conservation laws. At last, we show that the HARZ model enables us to investigate the effect of drivers with negative hysteresis loops on the traffic jams: in this case, stop-and-go waves can indeed decay faster than when the above chord-above-scanning condition fails. Furthermore, a lower ratio of positive hysteresis drivers versus negative ones is more likely to give the decay of speed oscillations. Indeed, it was discovered in Ref. 23 that a higher ratio is linked to the growth of such oscillations.

Section 9 draws some conclusions, while Appendix A contains the technical details concerning the numerical simulations.

2 | A BRIEF REVIEW OF THE ARZ MODEL

In the following, we almost always consider models in Lagrange coordinates; this makes the analysis simpler. To this aim, for $\rho > 0$ we introduce the spacing $u := 1/\rho$ and the velocity $w := v + p(\rho)$; we also denote $\tilde{p}(u) = p(\rho)$. Since we can assume that $\rho \leq \rho_{\max} = 1$ after normalization, then $u \geq 1$. We pass to Lagrange coordinates by making the change of variables

$$\tilde{x} = \int_{-\infty}^{x} \rho(\xi, t)\, d\xi.$$

Then, system (2) becomes

$$\begin{cases} u_t - v(u, w)_x = 0, \\ w_t = 0 \end{cases} \tag{3}$$

for

$$v(u,w) := w - p(u), \tag{4}$$

where we dropped the tildes both for x and p. The variable $w > 0$ is a kind of "Lagrangian marker" because it moves with the flow and so characterizes drivers. Because of (4) and (5), w can be understood as the maximum speed for drivers in the class w. One usually assumes

$$p(u) > 0, \quad p'(u) < 0, \quad \text{and} \quad p''(u) > 0 \tag{5}$$

for every $u > 0$. According to Ref. 3, one may choose $p(u) = Cu^{-\gamma}$, for $\gamma > 0$. Assumptions (5) are equivalent, for every $u > 0$, to

$$v(u,w) < w, \quad v_u(u,w) > 0, \quad \text{and} \quad v_{uu}(u,w) < 0. \tag{6}$$

The eigenvalues of system (3) are $\lambda_1 = -v_u(u,w) = p'(u) < 0 = \lambda_2$; under (5), λ_1 is genuinely nonlinear and λ_2 is linearly degenerate. In the plane (u,w), the rarefaction curves of the first (second) family are the straight lines $w =$ const. ($u =$ const., respectively) and so system (3) is a Temple system.[38]

3 | THE HARZ MODEL

In this section, we introduce a hysteretic driving behavior into the ARZ model; this will lead to the HARZ model. Indeed, we do not rely on the specific velocity law (4) but allow more general dependences of v on w to take into account different driving behaviors (see Ref. 15). We also let the minimum value of u be possibly larger than 1, depending on w. For simplicity, we use Lagrange coordinates as in Section 2 and exploit an analogous notation; the extension to Euler coordinates is straightforward.

In real traffic flows, drivers' speed-spacing relations for acceleration and deceleration are different, as shown in Refs. 28, 29, 31–33; points on these two curves are joined by scanning curves. In our model, for w fixed, we denote by $v = v^A(u,w)$ the *acceleration curve* for the driver w, while $v = v^D(u,w)$ is the *deceleration curve*. When the spacing u is small, the inequality $v^D(u,w) > v^A(u,w)$ holds (see fig. 3 from Ref. 28 and Figure 1). Each vehicle's speed v can be anywhere in the range between $v^A(u,w)$ and $v^D(u,w)$.

To intuitively show how a hysteretic driving behavior arises and to introduce our notation, we make use of Figure 1; there, arrows indicate the directions in which the state (u,v) can change and $v_{\max}$ denotes the maximum velocity. Consider a driver w whose state (u,v) is at point a and is accelerating. Then, the driver's state move toward the point b along the acceleration curve $v = v^A(u,w)$; we say that w is in *acceleration mode*. The set

$$A := \left\{(x,t) \in \mathbb{R}\times\mathbb{R}_+ : v(x,t) = v^A(u,w),\ v_t(x,t) > 0\right\} \tag{7}$$

is the collection of (x,t)'s where the driver x is in acceleration mode at time t. In (7) and in the sequel, when not otherwise specified, functions such as v, u, w are understood as functions of (x,t); therefore, the notation $v(x,t) = v^A(u,w)$ stands for $v(x,t) = v^A(u(x,t), w(x,t))$ for some (u,w).

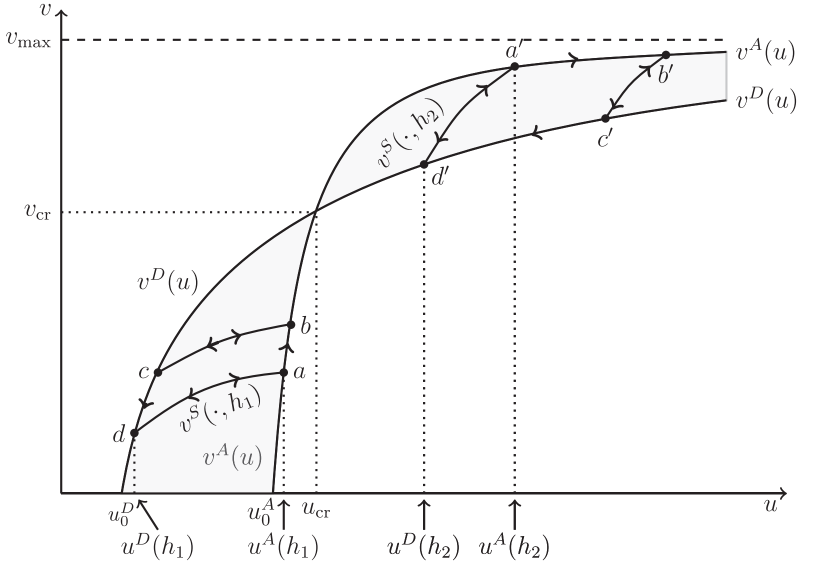

FIGURE 1 Speed-spacing relations $v^A = v^A(u, w)$, $v^D = v^D(u, w)$, and $v^S(u, w, h)$, with w *fixed*, for vehicles in acceleration, deceleration, and scanning mode, respectively. For simplicity, the dependence on w is dropped. Arrows indicate directions where the state of a vehicle can move. Note that the direction of the hysteresis loop $abcda$ and that of $a'b'c'd'a'$ are opposite: the counterclockwise loop $abcda$ can create stop-and-go waves, while the clockwise loop $a'b'c'd'a'$ depresses speed oscillations (see Ref. 34).

At b, if the driver has to decelerate due to tightening of spacing u, the state (u, v) cannot move backward along the curve $v = v^A(u, w)$ but it moves along the *scanning curve* bc, connecting the points b and c; this is due to either mental inertia or not wanting to lose momentum and hoping the spacing tightening is temporary. If u keeps decreasing, then the driver slowly decelerates to the point c. After that, possibly the driver has to decelerate faster for safety along the *deceleration curve* $v = v^D(u, w)$ toward d: the driver enters into *deceleration mode*. The set

$$D := \{(x, t) \in \mathbb{R} \times \mathbb{R}_+ : v(x, t) = v^D(u, w),\ v_t(x, t) < 0\} \tag{8}$$

denotes the (x, t)'s where deceleration mode occurs.

If the spacing u starts increasing at d, then the driver accelerates. At this point, the driver is not sure whether the improvement of spacing u is for real or temporary, and hence the driver will not accelerate stiffly along the deceleration curve $v = v^D(u)$, but gradually along the scanning curve da toward the point a. The loop $abcda$ is called a *hysteresis loop*.

The discussion above was focused in a region where $v^A(u) < v^D(u)$ and led to the formation of counterclockwise loops; in the case $v^A(u) > v^D(u)$ one argues analogously and sees the formation of clockwise loops. We refer to the following for the general case where the two cases occur together. For fixed w, the mutual position of the curves $u \mapsto v^A(u)$ and $u \mapsto v^D(u)$ represented in Figure 1 was deduced by Ref. 30 from experimental data in Ref. 28.

Now, we focus on the region between the acceleration and deceleration curves. When a driver is neither in acceleration nor deceleration mode, then the state moves along a scanning curve and we say the driver is in *scanning mode*. For a driver w, each scanning curve is identified by a parameter h which is constant along it. The equation for a scanning curve is then $v = v^S(u, w, h)$.

For example, on a scanning curve we can make the following choice:

$$\begin{aligned}&h \text{ is the } u\text{-coordinate of the intersection point of the scanning}\\ &\text{curve } v = v^S(u,w,h) \text{ with the deceleration curve } v = v^D(u,w).\end{aligned} \tag{9}$$

Such a u-coordinate is denoted as $u^D(w,h)$. The u-coordinate $u^A(w,h)$ is defined analogously by referring to the acceleration curve $v = v^A(u,w)$. These u-coordinates are the lower and upper boundary of the range of u for the given w and h: $u^D(w,h) \le u \le u^A(w,h)$ when the state moves on the h-scanning curve. For w fixed, the inverse function of $u = u^D(w,h)$ (or $u = u^A(w,h)$) is expressed as $h = h^D(u,w)$ and $h = h^A(u,w)$, respectively. For the example of parameterization of the scanning curves provided in (9), we have $u^D(w,h) = h$ and $h^D(u,w) = u$. The scanning set is defined as

$$S := \{(x,t) \in \mathbb{R} \times \mathbb{R}_+ \,:\, (x,t) \notin A \cup D\}. \tag{10}$$

Let the function $h = h(x,t)$ denote the scanning speed curve $v = v^S(u,w,h)$ the driver at (x,t) will take if the driver enters into the scanning mode. According to the description above, $h(x,t)$ should be either $h^A(u,w)$ or $h^D(u,w)$ according to the driver at (x,t) is in acceleration or deceleration mode; moreover, h is constant in the scanning mode. We point out that in Refs. 29, 33 the scanning curves are assumed to be horizontal, so that only the spacing changes while the velocity does not; as in Ref. 34, we generalize their modeling by dropping this restriction.

Since we have introduced our notation, we can finally write the HARZ model as

$$\begin{cases} u_t - v(u,w,h)_x = 0,\\ w_t = 0,\\ h_t = \chi^A(x,t)h^A(u,w)_t + \chi^D(x,t)h^D(u,w)_t, \end{cases} \tag{11}$$

where

$$v(u,w,h) := \begin{cases} v^D(u,w) & \text{if } u \le u^D(w,h),\\ v^S(u,w,h) & \text{if } u^D(w,h) < u < u^A(w,h),\\ v^A(u,w) & \text{if } u \ge u^A(w,h). \end{cases} \tag{12}$$

The functions χ^A and χ^D are the characteristic functions of the sets A and D, respectively, which are parts of the solution of system (11). For technical reasons, we extended by continuity v to $u < u^D(w,h)$ and $u > u^A(w,h)$. This in no way affects the properties of the model.

Now, we make precise the previous introduction of the model by stating the assumptions on the functions v^D, v^S, v^A and on the parameterization of the scanning curves. These hypotheses are consistent with what depicted in Figure 1.

We assume that we are given two constant values $w_{\min} \le w_{\max}$ and two functions $h_{\min}(w) \le h_{\max}(w)$ depending on the parameterization of the scanning curves, for every $w \in [w_{\min}, w_{\max}]$. Indeed, we let w vary in an interval just for simplicity; w could even take on only a finite number of values, leading to minor modifications in the following. We also consider two functions $v^A(u,w)$ and $v^D(u,w)$.

We denote by Ω the closed region in the (u, w, h)-space where

$$w \in [w_{\min}, w_{\max}], \quad h \in [h_{\min}(w), h_{\max}(w)], \quad u^D(w, h) \le u \le u^A(w, h). \tag{13}$$

As a consequence, in Ω we have v between $v^A(u, w)$ and $v^D(u, w)$. We also denote by Ω_w the section of Ω at fixed w. We now make some general assumptions.

Assumption 1.

(i) The functions $v^D(u, w)$ and $v^A(u, w)$ are defined for $w \in [w_{\min}, w_{\max}]$, and for either $u \ge u_0^D(w)$ or $u \ge u_0^A(w) > u_0^D(w)$, for some $u_0^D(w)$, $u_0^A(w)$, respectively.
Moreover, $v^D\left(u_0^D(w), w\right) = 0$ and $v^D(u, w) \le v_{\max}$, $v^A(u, w) \le v_{\max}$, for some $v_{\max} > 0$ independent of u, w, and h.
(ii) For every $w \ge 0$, there exists a unique $u_{cr} = u_{cr}(w) > u_0^A$ such that $v^D(u_{cr}, w) = v^A(u_{cr}, w)$; moreover, we have $v^D(u, w) > v^A(u, w)$ if $u_0^A < u < u_{cr}(w)$ and $v^A(u, w) > v^D(u, w)$ if $u > u_{cr}(w)$.
(iii) The scanning curves form a two-parameter family of curves

$$\left\{\left(u, v^S(u, w, h)\right)\right\}_{w \in [w_{\min}, w_{\max}],\ h \in [h_{\min}(w), h_{\max}(w)]}.$$

They cover the region Ω and, for every fixed $w \ge 0$, they are transverse to the curves $v = v^A$ and $v = v^D$.

The assumption that $v_{\max}$ does not depend on w in (i) above is different from the ARZ model[3,4] and it is only made for simplicity. The regions in the (u, v)-plane where $v < v_{cr}$ or $v > v_{cr}$ are called *congested* and *free* zones, respectively. We refer to Ref. 34 for a motivation to this terminology.

Some specific assumptions on the above functions now follow.

Assumption 2. The functions $h_{\min}(w)$ and $h_{\max}(w)$ are continuous; the functions $v^D(u, w)$, $v^A(u, w)$, and $v^S(u, w, h)$ are of class C^1 and satisfy in Ω the following conditions:

(i) $v_u^A > 0$, $v_u^D > 0$, $v_u^S \ge 0$;
(ii) $v_h^S > 0$;
(iii) $u_h^A > 0$, $u_h^D > 0$;
(iv) $u^A(w, h) > u^D(w, h)$, if $h \ne h_{cr}$ and $u^A(w, h_{cr}) = u^D(w, h_{cr})$;
(v) $\lim_{u\to\infty} v^A(u, w) = \lim_{u\to\infty} v^D(u, w) = v_{\max}$ for every $w \in [w_{\min}, w_{\max}]$.

Assumption (i) encodes the fact that, in Euler coordinates, the velocity is a decreasing function of the density; the function $u \mapsto v(u, w, h)$ in (12) is then Lipschitz-continuous and increasing. Assumption (ii), which clearly implies $v^S(u, w, h_1) \ne v^S(u, w, h_2)$ if $h_1 \ne h_2$, reflects the fact that the scanning curves do not intersect and the parameterization assigns higher values of h to higher scanning curves; this is in accord with the choice (9) of the parameterization. Such an assumption guarantees the unique covering of the set Ω by scanning curves. Assumptions (i) and (iii) imply $h_u^A > 0$, $h_u^D > 0$. Assumption (iii) is clearly compatible with Assumption (ii). In (iv), we denoted by $h_{cr} = h_{cr}(w)$ the value of the parameter h corresponding to u_{cr}; it exists because of (iii). As a consequence, we can define

$$v_{\rm cr}(w) := v(u_{\rm cr}(w), w, h_{\rm cr}(w)).$$

Assumption (iv) is satisfied by the parameterization in (9). Assumption (v) makes every driver travel at almost the maximum legal speed (which is independent of w) for large enough spacing u. It has an important consequence: it prevents "vacuum" states to occur between two adjacent vehicles to ensure the solvability of Riemann problem in Lagrange coordinates.

Remark 1. For most of our results, we need no further information on the dependence of the acceleration and deceleration curves on w. Indeed, we can assign w a physical interpretation; namely, it could represent the "aggressiveness" or "timidity" of a driving style. For example, for the same spacing u, an aggressive driver will drive faster than a timid one, meaning

$$v^A(u, w_{\rm tim}) < v^A(u, w_{\rm aggr}) \quad \text{and} \quad v^D(u, w_{\rm tim}) < v^D(u, w_{\rm aggr}),$$

where $w_{\rm tim}$ and $w_{\rm aggr}$ are the values of the w parameter for some timid and aggressive drivers, respectively. As a consequence, in the plane (u, v) the set $\Omega_{w_{\rm tim}}$ lies on the right of the set $\Omega_{w_{\rm aggr}}$ (see Figure 8 on the left). An analogous interpretation is done in Refs. 29, 33, but without referring to the ARZ model.

The eigenvalues of the homogeneous part of system (11) are v_u, which is genuinely nonlinear because of Assumption 2(i), and 0, which is double and linearly degenerate. Then, system (11) can be thought as a "generalized" Temple system.

4 | THE HARZ MODEL IN EULER COORDINATES

For completeness, in this section we briefly reformulate the HARZ model in Euler coordinates; in this case the variable x marks the position on the road. With a slight abuse of notation, we still use the same letters exploited in Lagrange coordinates to denote the corresponding quantities in Euler coordinates; we refer to Figure 2.

The acceleration, deceleration, and scanning velocities $v^A(u, w)$, $v^D(u, w, h)$, and $v^S(\rho, w, h)$ become $v^A(\rho, w)$, $v^D(\rho, w)$, and $v^S(\rho, w, h)$. As a consequence, the sets A, D, and S are now defined as

$$A := \left\{(x,t) \in \mathbb{R} \times \mathbb{R}_+ : v(x,t) = v^A(\rho, w),\ v_t(x,t) > 0\right\},$$
$$D := \left\{(x,t) \in \mathbb{R} \times \mathbb{R}_+ : v(x,t) = v^D(\rho, w),\ v_t(x,t) < 0\right\},$$
$$S := \{(x,t) \in \mathbb{R} \times \mathbb{R}_+ : (x,t) \notin A \cup D\},$$

where now, for example, h stands for the ρ-coordinate of the intersection point of the scanning $v = v^S(\rho, w, h)$ with the deceleration curve $v = v^D(\rho, w)$. As for Lagrange coordinates, we denote by $\rho^D(w, h)$ that coordinate, and analogously we define $\rho^A(w, h)$. For w fixed, the inverse functions of $\rho = \rho^D(w, h)$ and $\rho = \rho^A(w, h)$ are denoted by $h = h^D(\rho, w)$ and $h = h^A(\rho, w)$, respectively. If h is defined as above, then we have $\rho^D(w, h) = h$ and $h^D(\rho, w) = \rho$. We can now define the velocity

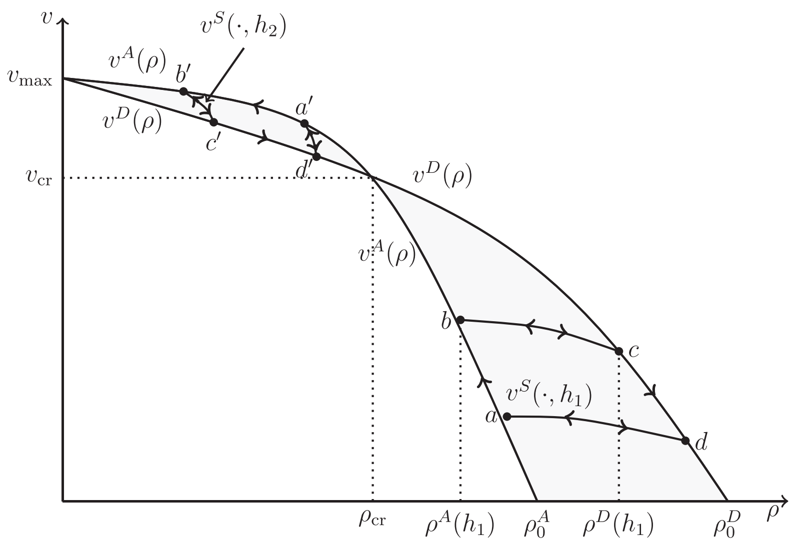

FIGURE 2 Speed–density relations $v^A = v^A(\rho, w)$, $v^D = v^D(\rho, w)$, and $v^S(\rho, w, h)$, with w *fixed*, for vehicles in acceleration, deceleration, and scanning mode, respectively. The dependence on w is omitted. Notation reflects that of Figure 1.

as

$$v(\rho, w, h) := \begin{cases} v^A(\rho, w) & \text{if } \rho \le \rho^A(w, h), \\ v^S(\rho, w, h) & \text{if } \rho^A(w, h) < \rho < \rho^D(w, h), \\ v^D(\rho, w) & \text{if } \rho \ge \rho^D(w, h). \end{cases}$$

Then, the HARZ model in Euler coordinates becomes

$$\begin{cases} \rho_t + (\rho v(\rho, w, h))_x = 0, \\ (\rho w)_t + (\rho v(\rho, w, h) w)_x = 0, \\ h_t + v h_x = \chi^A \left(h^A(\rho, w)_t + v h^A(\rho, w)_x \right) + \chi^D \left(h^D(\rho, w)_t + v h^D(\rho, w)_x \right), \end{cases} \tag{14}$$

where $\chi^A = \chi^A(x, t)$ and $\chi^D = \chi^D(x, t)$ are the characteristic functions of the sets A and D, respectively. System (14) is written in conservation form; otherwise, the second equation can be simply written as $w_t + v w_x = 0$. The reformulation of Assumptions 1 and 2 is straightforward and we leave it to the reader; we only point out that the congested and the free region (for fixed w) are again the regions in the (ρ, v)-plane where $v < v_{\text{cr}}(w)$ or $v > v_{\text{cr}}(w)$, respectively.

5 | The VISCOUS HARZ MODEL AND A PRIORI ESTIMATES

The general viscous version of system (11) is

$$\begin{cases} u_t - v(u, w, h)_x = \epsilon (B(u, w, h) v_x)_x, \\ w_t = 0, \\ h_t = \chi^A(x, t) h^A(u, w)_t + \chi^D(x, t) h^D(u, w)_t, \end{cases} \tag{15}$$

where B is smooth and

$$B(u, w, h) \geq \mu \tag{16}$$

for some real number $\mu > 0$. Notice the diffusion term, which slightly differs from that in Ref. 34; it is motivated by the following point of view of a vehicle driver. Think of $v(u, w, h)$ as an equilibrium speed. If the speeds of the vehicles in front of xth driver are faster the further ahead, that is, $v_x > 0$, then the driver, anticipating a faster speed, will drive a little faster than the steady-state speed. Then, the xth vehicle's speed will be $v = v(u, w, h) + \epsilon B v_x$ for some $\epsilon > 0$ and $B > 0$. An analogous argument applies in the case $v_x < 0$. Using this revised speed in (11) produces Equation $(15)_1$.

Due to the jump discontinuities of the coefficients in Equation $(15)_3$, the best smoothness one can hope for a typical solution of (15) is the Lipschitz continuity. Similarly to Ref. 39, consider the function space $\mathcal{PC}^2(\mathbb{R} \times [0, T]; \mathbb{R})$, which consists of the collection of piecewise C^2 functions $f : \mathbb{R} \times [0, T] \mapsto \mathbb{R}$. Here, piecewise C^2 means that $\mathbb{R} \times [0, T]$ can be partitioned locally into finitely many regions, with piecewise C^1 boundaries of the form $x = x(t)$, with finitely many pieces locally; the function $f(x, t)$ is C^2 in the interior of each region and can be extended as a C^2 function to the closure of each of them. Notice that if (u, w, h) is a solution to (15), then u_t is continuous in any open region where $v \in C^2$.

We now provide a min–max principle for the function v; see also Ref. 39 for a similar result. In view of Theorem 1, we consider functions satisfying the following assumptions, for some constant $v_\pm$:

$$u, w, h \in \mathcal{PC}^2(\mathbb{R} \times [0, +\infty)) \text{ and } v = v(u, w, h) \text{ is continuous;} \tag{17a}$$

$$v \text{ is either periodic in } x \text{ or satisfies } \lim_{x\to\pm\infty} v(x, t) = v_\pm. \tag{17b}$$

If u, h, and v satisfy (17a), then clearly $v \in \mathcal{PC}^2(\mathbb{R} \times [0, +\infty))$. For functions satisfying (17), we introduce the notation

$$L[u, v] := \epsilon v_{xx} + v_x - u_t, \qquad M(t) := \sup_{x\in\mathbb{R}} v(x, t). \tag{18}$$

Since $v(x, t)$ is continuous, then $M(t)$ is also continuous. Furthermore, under the boundary condition

$$v(\pm\infty, t) = v_\pm, \tag{19}$$

the inequality $M(t) \geq v_\pm$ is automatically satisfied because of (17b).

Lemma 1. *Assume (17) and $v_u^S > 0$. If $L[u, v] > 0$ for all $(x, t) \in \mathbb{R} \times [0, T]$, then $M(t) \leq M(0)$ for all $t \in [0, T]$.*

Proof. Assume, for contradiction, that $M(t_1) > M(0)$ at some $t_1 > 0$. Then, due to the continuity of $M(t)$, there is $0 < t_0 \leq t_1$ and some constant $\nu > 0$ such that

$$M(t_0) > M(0), \quad \text{and } M(t) < M(t_0) \quad \text{for } t_0 - \nu < t < t_0. \tag{20}$$

Due to continuity of $v(x,t)$ and (17b), there is a point x_0 such that

$$v(x_0,t_0) = M(t_0).$$

To get a contradiction, it suffices to show that

$$v_t(x_0,t_0-) < 0, \tag{21}$$

where we understand (21) as $v_t(x_0-,t_0-) < 0$ if v is not t-differentiable at x_0. Indeed, estimate (21) leads to $v(x_0,t) > v(x_0,t_0)$ over the interval $t_0-\nu < t < t_0$, adjusting for a smaller $\nu > 0$ if necessary. In turn, this implies $M(t) > M(t_0)$ over the interval $t_0-\nu < t < t_0$, contradicting (20).

Summarizing, the point x_0 is a local maximum point of the function $v(\cdot,t_0)$ and $v(x,t)$ is a $\mathcal{PC}^2$ function.

Case 1: (x_0,t_0) is inside a region where $v \in C^2$.

In this case, we have $v_x(x_0,t_0) = 0 \geq v_{xx}(x_0,t_0)$. From the condition $L[u,v] > 0$, we infer that $u_t(x_0,t_0) < 0$. Therefore, we deduce

$$v_t(x_0,t_0) = (v_u^A \text{ or } v_u^D \text{ or } v_u^S)(x_0,t_0)\, u_t(x_0,t_0) < 0,$$

because of either Assumption 2(i) or $v_u^S > 0$, which contradicts (20).

Case 2: (x_0,t_0) is on the boundary of regions where $v \in C^2$.

We recall that a $\mathcal{PC}^2$ function is of class C^2 apart from a finite number of curves of the form $x = x(t)$, where $x(t)$ is piecewise C^1. Therefore, in the current case, we have that (x_0-,t_0) and (x_0+,t_0) are in different C^2 regions. Thus, $v_x(x_0\pm,t_0)$ exists, since there are only finitely many C^1 boundaries locally.

Since x_0 is a local maximum point of $v(\cdot,t_0)$, the inequalities

$$v_x(x_0-,t_0) \geq 0 \geq v_x(x_0+,t_0) \tag{22}$$

are satisfied. We have two subcases.

First, assume that one of the equalities in (22) is broken, so that

$$v_x(x_0+,t_0) - v_x(x_0-,t_0) < 0.$$

Consider a test function $\phi(x) \in C_c^\infty(\mathbb{R})$, with support in the interval $(x_0-\mu, x_0+\mu)$, which satisfies $\phi(x_0) = 1$, $(x-x_0)\phi_x(x) \leq 0$, and $\int \phi\, dx = \mu$. Then, in the sense of distributions, the assumption $L[u,v] > 0$ implies

$$\begin{aligned}
\langle u_t, \phi\rangle < \langle v_x + v_{xx}, \phi\rangle &= -\int_{x_0-\mu}^{x_0+\mu} (v+v_x)\phi_x(x)\,dx \\
&= -\int_{x_0-\mu}^{x_0+\mu} (v(x_0,t_0) + O(1)(x-x_0))\phi_x(x)\,dx \\
&\quad - \int_{x_0-\mu}^{x_0} (v_x(x_0-,t_0) + O(1)(x-x_0))\phi_x(x)\,dx \\
&\quad - \int_{x_0}^{x_0+\mu} (v_x(x_0+,t_0) + O(1)(x-x_0))\phi_x(x)\,dx
\end{aligned}$$

$$= O(1)\int_{x_0-\mu}^{x_0+\mu}(x-x_0)\phi_x(x)\,dx + [v_x(x_0+,t_0) - v_x(x_0-,t_0)]\phi(x_0)$$

$$= O(1)\mu + [v_x(x_0+,t_0) - v_x(x_0-,t_0)] < 0. \tag{23}$$

This implies $u_t(x_0,t_0) < 0$ in the sense of distributions, which contradicts (20), arguing as in Case 1. Notice that estimates (23) are still true when $L[u,v] = 0$; this will be used in Theorem 1.

The only remaining possibility is that both equalities in (22) holds. In this situation, $v_{xx}(x_0\pm,t_0) \le 0$ must happen at the local maximum point x_0. Then, $L[u,v] > 0$ implies $u_t(x_0,t_0) < 0$ in the sense of distribution and hence still contradicts (20). □

Theorem 1. *Assume (15) has a solution $(u,w,h)(x,t)$ satisfying (17), and $v_u^S > 0$. If, for every $t \ge 0$, the function $v(u,w,h)(\cdot,t)$ is not constant over any nonempty interval, then the estimates*

$$\inf_{x\in\mathbb{R}} v(x,0) \le v(x,t) \le \sup_{x\in\mathbb{R}} v(x,0) \tag{24}$$

hold for $(x,t) \in \mathbb{R}\times[0,\infty)$.

Proof. For sake of simplicity, we assume $B = 1$; the general case can be treated with minor modifications. A solution $(u,h,v = v(u,w,h))\,(x,t)$ of (15) satisfies

$$L[u,v] = v_x + \epsilon v_{xx} - u_t = 0.$$

We intend to show that $M(t) \le M(0)$ for $t > 0$; the proof of the inequality on the left in (24) is entirely similar. As in the proof of Lemma 1, assume, for contradiction, that there is a $t_0 > 0$ such that (20) holds. It follows from (17b) that

$$x_0 := \operatorname*{argmax}_{x\in\mathbb{R}} v(x,t_0) \in \mathbb{R}. \tag{25}$$

We claim that (20) and (25) are contradictory, shown as follows.

Case 1: (x_0,t_0) is inside a region where $v \in C^2$. In this case, we have

$$v_x(x_0,t_0) = 0 \ge v_{xx}(x_0,t_0). \tag{26}$$

Since the function $v(\cdot,t_0)$ cannot be constant over any interval, there are two points $x_l < x_r$, with $x_l < x_0 < x_r$ and $x_r - x_l < \epsilon/2$, such that

$$v(x_0,t_0) > v(x_l,t_0) \quad \text{and} \quad v(x_0,t_0) > v(x_r,t_0). \tag{27}$$

Then, (20) and (27) ensure that

$$v(x_0,t_0) > \max\{v(x_l,t),v(x_r,t),v(x,t_0-\nu)\} \quad \text{for} \quad x\in[x_l,x_r],\ t_0-\nu \le t \le t_0. \tag{28}$$

We denote (see Figure 3)

$$D_\nu := [x_l,x_r]\times[t_0-\nu,t_0]. \tag{29}$$

We have $L[u,v] = 0$ in D_ν, and $v(x_0,t_0) > v$ at left, right, and bottom sides of ∂D_ν. If it were $L[u,v] > 0$ in D_ν, then the arguments of Lemma 1 could be used to show that the maximum value

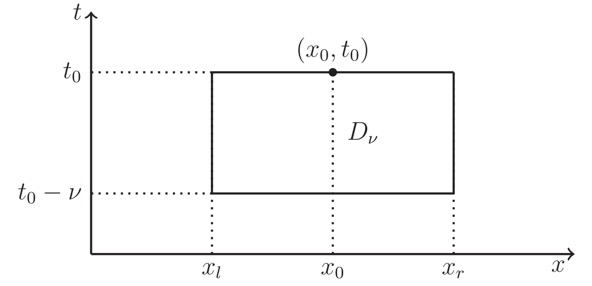

FIGURE 3 The region D_ν.

of v cannot occur at an interior point of the upper boundary of D_ν, such as (x_0, t_0). To reuse the arguments in the proof of Lemma 1, consider the auxiliary function

$$V(x,t) := v(x,t) + \mu(x - x_0)^2 \tag{30}$$

with the constant $\mu > 0$ chosen small enough so that (28) still holds after replacing v by V:

$$\begin{aligned} V(x_0,t_0) &= v(x_0,t_0) \\ &> \max\{V(x_l,t), V(x_r,t), V(x,t_0-\nu)\} \text{ for } x \in [x_l, x_r],\ t_0 - \nu \le t \le t_0. \end{aligned} \tag{31}$$

This is achievable because v is continuous and the set ∂D_ν is compact. For this V, the inequality

$$\begin{aligned} L[u,V] = \epsilon V_{xx} + V_x - u_t &= 2\epsilon\mu + 2\mu(x - x_0) \\ &> 2\epsilon\mu - 2\mu(x_r - x_l) > 2\mu(\epsilon - \epsilon/2) > 0 \end{aligned} \tag{32}$$

is true for $(x,t) \in D_\nu$. Thus, the function V cannot exceed its initial-boundary values on D_ν. This contradicts (31), and therefore Case 1 cannot happen.

Case 2: The point (x_0,t_0) is at a boundary between regions where $v \in C^2$.

As in Case 2 of the proof of Lemma 1, we have (22), and consider the following subcases.

Subcase 2(i): $v_x(x_0+, t_0) \neq v_x(x_0-, t_0)$. Note that the proof of (23) still works when $L[u,v] = 0$, leading to $u_t(x_0,t_0) < 0$, which contradicts (20).

Subcase 2(ii): $v_x(x_0-, t_0) = v_x(x_0+, t_0) = 0$. In this case, it is necessary that $v_{xx}(x_0\pm, t_0) \le 0$. Then the arguments from (26) to (32) still work, in the sense of distribution, to yield $u_t < 0$ and hence a contradiction again.

In all cases, there is a contradiction between (20) and (25). The proof is complete. □

Remark 2. We denote by TV the total variation of a function of the variable x. We show with *formal* arguments that if $(u,w,h)(x,t)$ is a solution of (15) with sufficiently smooth v, then

$$\mathrm{TV}\,(v(\cdot,t_1)) \ge \mathrm{TV}\,(v(\cdot,t_2)) \quad \text{for } 0 \le t_1 < t_2. \tag{33}$$

To this aim, we denote by v^* any of the functions v^A, v^S, or v^D. Recall that every solution satisfies $w_t = 0$ and $h_t = 0$ along the scanning curves; hence we deduce

$$\begin{aligned} \frac{d}{dt}\mathrm{TV}\,(v(\cdot,t)) &= \frac{d}{dt}\int_{\mathbb{R}} |v_x(x,t)|\,dx = \int_{\mathbb{R}} [\mathrm{sign}(v_x)_t v_x(x,t) + \mathrm{sign}(v_x) v_{xt}]\,dx \\ &= \int_{\mathbb{R}} \mathrm{sign}(v_x)[v_u^* u_t]_x\,dx = -\int_{\mathbb{R}} \mathrm{sign}(v_x)_x [v_u^*(v_x + \epsilon v_{xx})]\,dx, \end{aligned} \tag{34}$$

$$= -\epsilon \int_{\mathbb{R}} \operatorname{sign}(v_x)_x v_u^* v_{xx}\, dx, \tag{35}$$

in the sense of distributions. In (34), we made use of

$$\operatorname{sign}(v_x)_t v_x = O(1) \sum_j \delta\big(x - x_j(t)\big) v_x = 0,$$

where $x = x_j(t)$ are the points across which $\operatorname{sign}(v_x)$ changes, and hence $v_x = 0$.

Furthermore, around each point x_0 where $\operatorname{sign}(v_x)$ changes, we have

$$\operatorname{sign}(v_x)_x v_{xx} = [\operatorname{sign}(v_x(x_0+)) - \operatorname{sign}(v_x(x_0-))]\delta(x - x_0) v_{xx}(x_0).$$

Omitting the dependence on t, if $\operatorname{sign}(v_x(x_0+)) - \operatorname{sign}(v_x(x_0-)) > 0$, then $v_{xx}(x_0) \geq 0$. Else, if $\operatorname{sign}(v_x(x_0+)) - \operatorname{sign}(v_x(x_0-)) < 0$, then $v_{xx}(x_0) \leq 0$. Either way, the inequality $\operatorname{sign}(v_x)_x v_{xx} \geq 0$ holds. Recalling that we have $v_u^* \geq 0$ by assumption, statement (33) follows from (35).

6 | BASIC WAVES OF HARZ MODEL

In this section, we find all basic waves of system (11) that are needed to construct its Riemann solver. As in Refs. 34, 39, in the case of discontinuous solutions of (11) we only admit the ones that have a viscous profile. Traveling waves of (15) are solutions of the form $(u(\xi), w(\xi), h(\xi))$, where $\xi := (x - st)/\epsilon$ and s is constant; they are also required to assume some given values at $\xi = \pm\infty$. More precisely, they satisfy the boundary-value problem

$$\begin{cases} -s(u - u_-) - (v - v_-) = B(u, w, h) v', \\ -s(w - w_-) = 0, \\ sh' = s\chi^A(\xi) h^A(u, w)' + s\chi^D(\xi) h^D(u, w)', \\ (u, w, h)(\pm\infty) = (u_\pm, w_\pm, h_\pm), \quad (u', w', h')(\pm\infty) = (0, 0, 0), \end{cases} \tag{36}$$

where $' = \frac{d}{d\xi}$ for some $(u_\pm, w_\pm, h_\pm) \in \Omega$. The speed s is determined by Equation $(36)_1$ at $\xi = \pm\infty$, namely,

$$s = -\frac{v_+ - v_-}{u_+ - u_-}, \tag{37}$$

where $v_\pm := v(u_\pm, w_\pm, h_\pm)$. If $s \neq 0$, solutions to (36) are meant as continuous functions. If $s = 0$, then Equations $(36)_2$ and $(36)_3$ impose no restrictions on both w and h; in this case Equation $(36)_1$ is trivially satisfied by $v(\xi) := v_-$ and any $w = w(\xi)$, $h = h(\xi)$.

Lemma 2. *A solution of system (36), valued in Ω, has $s = 0$ if and only if $v_- = v_+$. If $s \neq 0$, then both $w(\xi) \equiv w_- = w_+$ and $s < 0$ occur.*

Proof. The first statement is obvious from (37). About the second, it is clear from $(36)_2$ that if $s \neq 0$ then $w'(\xi) \equiv 0$, and hence $w(\xi) \equiv w_-$; as a consequence, we have $w_+ = w_-$. We have $v_u \geq 0$ by Assumption 2(i); then by (37) we deduce $s < 0$. □

In the case of the system in (36), the sets A, D, S defined in (7), (8), (10) become

$$A = \{\xi \in \mathbb{R} \ : \ v = v^A, v' > 0\},\ D = \{\xi \in \mathbb{R} \ : \ v = v^D, v' < 0\},\ S = (A \cup D)^{\complement}, \tag{38}$$

respectively, because $v_t = -sv'$. For $s = 0$, the sets A and B are empty.

For completeness, all available rarefaction waves and viscous shocks are listed below. The proof of their existence follows from this list.

(i) *Deceleration shocks* connect two states

$$\big(u_-, v_- = v^D(u_-, w_-)\big) \text{ and } \big(u_+, v_+ = v^D(u_+, w_+ = w_-)\big), \quad u_- > u_+,$$

on the deceleration curve $v = v^D(u, w_-)$. Note that there is no rarefaction wave connecting two states on $v = v^D(u, w_-)$.

(ii) *Acceleration rarefaction waves* along the acceleration curve $v = v^A(u, w_-)$ connect two states

$$\big(u_-, v_- = v^A(u_-, w_-)\big) \text{ and } \big(u_+, v_+ = v^A(u_+, w_+ = w_-)\big), \quad u_- < u_+.$$

There is no shock wave connecting two states on $v = v^A(u, w_-)$.

(iii) *Scanning waves* connect two states

$$(u_-, w_-, h_-) \text{ and } (u_+, w_+ = w_-, h_+ = h_-)$$

on the same scanning curve. If $u_- \le u_+$, then the scanning wave is a rarefaction wave; else, it is a shock.

(iv) *Acceleration shocks from scanning to acceleration mode*, connect two states

$$(u_-, w_-, h_-) \text{ and } (u_+, w_+, h_+) = \big(u_+ > u_-, w_-, h_+ = h^A(u_+, w_-) > h_-\big),$$

under the *chord-above-scanning* condition

$$-s = \frac{v_+ - v_-}{u_+ - u_-} > \frac{v(u, w_-, h_-) - v_-}{u - u_-}, \text{ for all } u_- < u < u_+. \tag{39}$$

(v) *Deceleration shocks from scanning to deceleration mode*, connect the states

$$(u_-, h_-, w_-) \text{ and } (u_+, h_+, w_+) = \big(u_+ < u_-, w_-, h_+ = h^D(u_+, w_-) < h_-\big),$$

under the *chord-below-scanning* condition

$$-s = \frac{v_+ - v_-}{u_+ - u_-} > \frac{v(u, h_-, w_-) - v_-}{u - u_-}, \text{ for all } u_- > u > u_+. \tag{40}$$

(vi) *Stationary shocks*, connect the states

$$(u_-, v_-, w_-) \text{ and } (u_+, v_+ = v_-, w_+).$$

These are the only wave allowing $w_- \neq w_+$ because of Lemma 2.

The first three kinds of waves are the usual Lax shock and rarefaction waves for scalar conservation laws with concave fluxes $v^A(u, w_-)$, $v^D(u, w_-)$, and $v^S(u, w_-, h_-)$. The nonexistence part of (i) and (ii) is due to the fact that such waves would violate Equation $(15)_3$. The scanning waves in (iii) cover the case when $h_- = h_+$. The existence of waves in (iv)–(vi) is a consequence of the results below.

To make clearer the analysis, we strengthen Assumption 2 as follows.

Assumption 3 (technical assumptions). The functions $v^A(u, w)$, $v^D(u, w)$, and v^S satisfy in Ω the following conditions:

(i) $v^A_{uu} < 0$, $v^D_{uu} < 0$;
(ii) $v^S_u > 0$ and $v^S_{uu} < 0$.

These assumptions make simple the identification of shock and rarefaction waves. For instance, along a deceleration (acceleration) curve we can only have shock (if we move down) or rarefaction waves (if we move up). Moreover, the assumption $v^S_{uu} < 0$ makes the chord-below-scanning assumption (40) always satisfied; this is not the case for the chord-above-scanning assumption (39), and this possibility shall play a key role in Section 8.

Remark 3. The definition (12) of $v(u, w, h)$, Assumptions 2(i) and 3(ii) imply that the function $v(u, w, h)$ is Lipschitz-continuous and strictly increasing in u; hence its inverse function $u = u(v, w, h)$ is well-defined. Furthermore, the function $u(v, w, h)$ is Lipschitz-continuous, because it is C^1 except at the two points where the curve $u \mapsto v^S(u, w, h)$ intersects the curves $u \mapsto v^A(u, w)$ and $u \mapsto v^D(u, w)$, respectively, due to Assumption 2. Using $u = u(v, w, h)$, we can regard (v, w, h) as unknown functions for the system (36), where u is understood as $u = u(v, w, h)$.

Lemma 3. *If $(v, w, h)(\xi)$ is a solution for $\xi \in \mathbb{R}$ of system (36), with $s \neq 0$, then $v'(\xi) \neq 0$ for any $\xi \in \mathbb{R}$.*

Proof. Notice that v is of class C^1 because of (16) and since we are considering continuous functions as solutions. Moreover, by Lemma 2 we have $w(\xi) \equiv w_- = w_+$.

Assume, by contradiction, that $v'(\xi_0) = 0$ for some $\xi_0 \in \mathbb{R}$. Then $(36)_1$ implies

$$-s(u_0 - u_-) - (v_0 - v_-) = 0, \tag{41}$$

where $(u_0, v_0, h_0) := (u, v, h)(\xi_0)$.

Since $v_- \neq v_+$ by (37) and $s \neq 0$, then either $v(\xi_0) = v_-$ or $v(\xi_0) = v_+$ must fail. Assume $v(\xi_0) \neq v_+$; the proof for the other case is similar. Then, there exists $\xi_1 > \xi_0$ such that $v'(\xi_1) \neq 0$; by the continuity of v' we have, for some $\nu_0 > 0$,

$$v'(\xi) \neq 0 \quad \text{for } \xi \in [\xi_1, \xi_1 + \nu_0). \tag{42}$$

We claim that (41) implies $v(\xi) \equiv v_0$, which contradicts (42). To this end, we note that (36), because of (41), leads to

$$\begin{cases} -s[u - u_0] - (v - v_0) = B(u, w_-, h)(v - v_0)', \\ (h - h_0)' = \chi^A(\xi)\big[h^A(u, w_-) - h_0\big]' + \chi^D(\xi)\big(h^D(u, w_-) - h_0\big)'. \end{cases} \tag{43}$$

Recall that $h^D(u, w_-)$ is the h-value of the point $\left(u, v^D(u, w_-)\right)$. This point coincides with $\left(u^D(v, w_-), v\right)$, whose h-value is then also a function of (v, w_-). With a slight abuse of notation, we use $h^D(v, w_-)$, $h^A(v, w_-)$ in (43) instead of $h^D(u, w_-)$, $h^A(u, w_-)$. Remembering Remark 3, then (43) implies

$$B(u(v, w_-, h))(v - v_0)' = O(1)(v - v_0).$$

Integrating this equation over the interval $[\xi_1, \xi_1 + \nu]$, for $0 < \nu < \nu_0$, yields

$$\mu|v(\xi) - v_0| \leq O(1)\, \nu \max_{\xi \in [\xi_1, \xi_1 + \nu]} |v(\xi) - v_0|.$$

This cannot be true for $\nu > 0$ sufficiently small unless $v(\xi) \equiv v_0$ for $\xi \in (\xi_1, \xi_1 + \nu)$. This contradicts (42) and proves the lemma. $\square$

Remark 4. Under the assumption of Lemma 3, the function $u = u(\xi)$ is Lipschitz-continuous. By definition (9) and Assumption 2(i), it also follows that $h = h(\xi)$ is Lipschitz-continuous.

Case (iii) covers the case when $h_- = h_+$; in this case system (11) is reduced to a single conservation law with strictly concave flux (by Assumption 3(ii), and then the existence of viscous profiles when $u_- > u_+$ is classical.[38] Therefore, we only consider the case $h_+ \neq h_-$ in what follows.

Theorem 2 (Existence and uniqueness of scanning-to-acceleration shocks). *Assume $(u_\pm, w_- = w_+, h_\pm) \in \Omega$, $h_+ \neq h_-$, and $v_+ > v_-$. Then, there is a solution of system (36) if and only if $h_+ > h_-$, $v_+ = v^A(u_+, w_+)$ and the chord-above-scanning condition (39) is satisfied. Furthermore, the solution must be of the form*

$$(v, h)(\xi) := \begin{cases} (v(\xi), h_-) & \text{if } \xi \leq \xi_0, \\ \left(v(\xi), h^A(v(\xi), w_-)\right) & \text{if } \xi > \xi_0, \end{cases} \tag{44}$$

and hence is unique up to a shift. Here, the point ξ_0 is uniquely defined by $v(\xi_0) = v^A\left(u^A(w_-, h_-), w_-\right)$.

Proof. We notice that from the assumption $v_+ > v_-$ and (37) it follows $s \neq 0$. Thus, if v is a solution, then $v'(\xi) > 0$ for all $\xi \in \mathbb{R}$ by Lemma 3, implying $\xi \notin D$. Then, h cannot decrease as ξ increases, and the assumption $h_+ \neq h_-$ leads to $h_+ > h_-$. We refer to Figure 4 for the graph of the function $v(\cdot, w_-, h_-)$ and the relative positions of $(u_\pm, v_\pm)$.

We first prove the sufficient part of the statement. Recall (36), Remark 3, and consider the problem

$$\begin{cases} B(u(v, w_-, h_-))v' = -s(u(v, w_-, h_-) - u_-) - (v - v_-), \\ v(\pm\infty) = v_\pm. \end{cases} \tag{45}$$

Equation $(45)_1$ can be written as

$$B(u(v, w_-, h_-))v' = \left(-s\frac{u(v, w_-, h_-) - u_-}{v - v_-} - 1\right)(v - v_-). \tag{46}$$

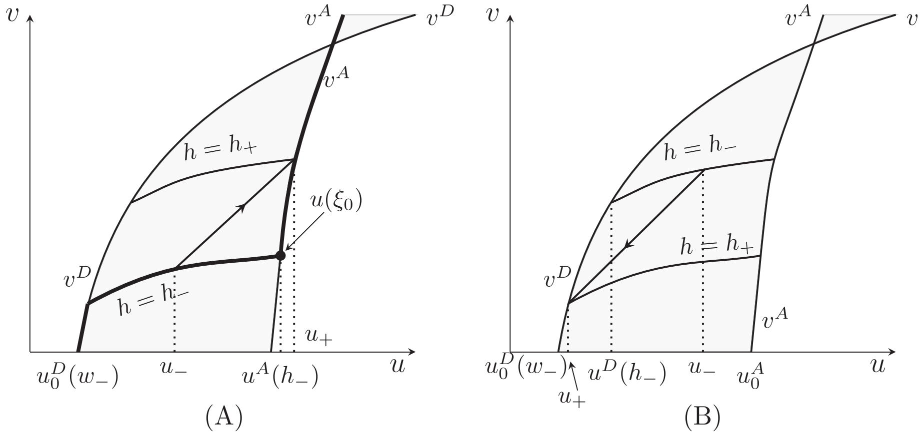

FIGURE 4 The $(u_\pm, v_\pm)$ states that can be connected by (A) a scanning-to-acceleration shock, and (B) a scanning-to-deceleration shock. The thick curve in (A) is $v = v(u, w_-, h_-)$.

Pick any v_0 in the interval (v_-, v_+) and let $v = v(\xi)$ be the solution to Equation (46) with initial condition $v(0) = v_0$. Since the term in the big parentheses in $(46)_1$ is positive over the range $v_- < v < v_+$, because of the chord-above-scanning condition (39), then $v(\xi)$ increases to v_+ as $\xi \to \infty$. Analogously, we have $v(\xi) \to v_-$ as $\xi \to -\infty$.

This shows that problem (45) has a solution $v(\xi)$, with $v'(\xi) > 0$ for every $\xi \in \mathbb{R}$. Hence, the function

$$u(\xi) := u(v(\xi), w_-, h_-) \tag{47}$$

also satisfies $u'(\xi) > 0$ for every $\xi \in \mathbb{R}$, with the possible exception of the two values of ξ such that $u(\xi) = u^D(w_-, h_-)$ or $u(\xi) = u^A(w_-, h_-)$, where u has a jump discontinuity. We have $u_- \leq u_A(w_-, h_-)$ and $u^+ > u^A(w_-, h_-)$, because $h_+ > h_-$; then there exists a unique $-\infty \leq \xi_0 < \infty$ such that $u(\xi) = u^A(w_-, h_-)$ (see Figure 4A). Define

$$h(\xi) := \begin{cases} h_- & \text{if } \xi \leq \xi_0, \\ h^A(u(\xi), w_-) & \text{if } \xi > \xi_0. \end{cases} \tag{48}$$

We now prove that the function $(u, w_-, h)(\xi)$ is a solution of problem (36).

Equation $(36)_1$ is satisfied by $(u, w_-, h)(\xi)$; in fact, $v\,(u(\xi), w_-, h(\xi))$ coincides with $v\,(u(\xi), w_-, h_-)$ both when $\xi \leq \xi_0$ (and then $h(\xi) = h_-$) and when $\xi > \xi_0$ (and then $h(\xi) = h^A\,(u(\xi), w_-) > h_-$) because of (12). Then, with the pair $(u, h)(\xi)$ constructed by (47) and (48), Equation $(36)_1$ is equivalent to $(45)_1$.

Equation $(36)_2$ is trivially satisfied for $\xi < \xi_0$ by $h(\xi) = h_-$, because in this case we have both $\xi \notin A$ and $\xi \notin D$. When $\xi > \xi_0$, Equation $(36)_2$ is still true because $h(\xi) = h^A\,(u(\xi), w_-)$ and $\xi \in A$. Note that $h(\xi)$ is continuous at $\xi = \xi_0$, although $(u', h')(\xi)$ may have a jump discontinuity at $\xi = \xi_0$. Then, $(u, w_-, h)(\xi)$ satisfies $(36)_2$ in the sense of distribution.

At last, the structure (44) of the solution follows from the above construction. This concludes the proof of the sufficient part of the statement.

To show the necessary part of the statement, assume (36) has a solution. Since $v_+ > v_-$, Lemma 3 states that $v'(\xi) > 0$ for all $\xi \in \mathbb{R}$. This and (45) imply (39). To see that $v_+ = v^A(u_+, w_-)$ is also necessary, note that because $h_+ > h_-$, there is a point $\xi_2 \in \mathbb{R}$ where $h'(\xi_2) > 0$ holds.

The function h can increase only if $\xi \in A$, and hence $v(\xi_2) = v^A(u(\xi_2), w_-)$. Since $v'(\xi) > 0$ for all $\xi \in \mathbb{R}$, if $v(\xi) = v^A(u(\xi), w_-)$ for some ξ, then $\xi \in A$ by (38). Then $(36)_3$ and $v'(\xi) > 0$, which implies $s \neq 0$, ensure that $h = h^A(u, w_-)$ and hence $v(\xi) = v^A(u(\xi), w_-)$ remains true as ξ increases. This, in the $\xi \to \infty$ limit, forces $h_+ = h^A(u_+, w_-)$ and hence $v_+ = v^A(u_+, w_-)$.

It remains to show that a solution of (36) must have the form (44). The necessity of the chord-above-scanning condition (39) excludes the possibility that (u_-, v_-) lies on the curve $v = v^A(u, w_-)$ because of the concavity of the acceleration curve $v^A(\cdot, w)$ required in Assumption 3(ii). This and $v' > 0$ lead to $\xi \in S$ for $\xi \ll -1$. Therefore, we have $(-\infty, \xi_0) \subseteq S$, for ξ_0 defined in the statement. Over this interval, $h(\xi) = h_-$ holds since h does not change in S-mode. The reason for the interval to terminate at ξ_0 is that $\xi_0 \notin S$ and hence $\xi_0 \in A$ because $v' > 0$. This implies $v(\xi_0) = v^A(u(\xi_0), w_-, h_-)$. This proves $(44)_1$. As ξ increases from ξ_0, since $v' > 0$ and $v(\xi_0) = v^A(u(\xi_0), w_-, h_-)$, Equation $(36)_3$ forces $h(\xi)$ to be $h^A(u(\xi), w_-)$, justifying $(44)_2$. The above reasoning allows to conclude that (44) is the only form of solutions for (36). The uniqueness of the solution of (36) follows. $\square$

Theorem 3 (Existence and uniqueness of scanning-to-deceleration shocks). *Assume $(u_\pm, w_- = w_+, h_\pm) \in \Omega$, $h_+ \neq h_-$, and $v_+ < v_-$. There is a solution of (36) if and only if $h_- < h_+$, $v_+ = v^D(u_+, w_+)$ and the chord-below-scanning condition (40) is satisfied. Furthermore, the solution must be of the form*

$$(v, h)(\xi) := \begin{cases} (v(\xi), h_-) & \text{if } \xi \le \xi_0, \\ \left(v(\xi), h^D(v(\xi), w_-)\right) & \text{if } \xi > \xi_0, \end{cases} \tag{49}$$

and hence is unique up to a shift. Here, ξ_0 is uniquely determined by $v(\xi_0) = v^D(u^D(h_-, w_-), w_-)$.

The proof of Theorem 3 is similar to that of Theorem 2, and hence is omitted. This concludes the discussion of cases (iv) and (v) above. We now consider case (vi).

Stationary shocks' speed s is 0, forcing $v_- = v_+$ in view of (37), but allows w to change. This makes (36) into

$$\begin{cases} B(u, w, h)v' = v_\pm - v, \\ (u, w, h)(\pm\infty) = (u_\pm, w_\pm, h_\pm), \ (u', w', h')(\pm\infty) = (0, 0, 0). \end{cases} \tag{50}$$

Theorem 4 (Existence of stationary shocks). *Given $(u_\pm, w_\pm, h_\pm) \in \Omega$ with $v_- = v_+$, there is a solution to (50).*

Proof. Any function $(u, w, h)(\xi)$ satisfying $v(u, w, h) \equiv v_-$ and $(u, w, h)(\pm\infty) = (u_\pm, w_\pm, h_\pm)$ can be a solution of (50). Consider, for example, the function

$$(u(\xi), w(\xi), h(\xi)) := \begin{cases} (u_-, w_-, h_-) & \text{if } \xi \le 0, \\ (u_+, w_+, h_+) & \text{if } \xi > 0. \end{cases} \tag{51}$$

By the assumptions of this theorem, we have $v\,(u(\xi), w(\xi), h(\xi)) \equiv v_\pm$ and then (51) trivially satisfies (50). $\square$

7 | RIEMANN SOLVERS OF THE HARZ MODEL

In this section, we construct a Riemann solver for the inviscid system (11). Each shock wave occurring in the solution is required to have a viscous traveling-wave profile, which is provided by Section 6; this avoids nonphysical solutions.

A Riemann solver of the system (11) is a solution $(u, w, h)(\xi)$, for $\xi = x/t$, of (11) satisfying the Riemann initial data

$$(u, w, h)(x, 0) = \begin{cases} (u_-, w_-, h_-) & \text{if } x < 0, \\ (u_+, w_+, h_+) & \text{if } x > 0, \end{cases} \tag{52}$$

with $(u_\pm, w_\pm, h_\pm) \in \Omega$. It consists of the basic waves listed in Section 6. We divide the discussion in some cases. Below, S denotes shock waves, R rarefaction waves, SS stationary shock waves, ScS scanning shock waves, ScR scanning rarefaction waves, AR acceleration rarefaction waves, DS deceleration shocks, and ScDS scanning-to-deceleration and ScAS scanning-to-acceleration shocks.

Theorem 5. *The Riemann problem for system (11) with initial data (52) in Ω has a solution in Ω, which is formed by the waves described in Section 6. Moreover, for such a solution the velocity v is monotone, and it is unique among the solutions with this property. It is given by (55), (56), (58), and (59).*

Proof. We first construct the solution. The state variables are (u, w, h); however, for clarity, we also show below the velocity. We denote by $(v^S)^{-1}(v, w, h)$ the inverse function of the function $u \mapsto v^S(u, w, h)$ for w, h fixed. An analogous notation is used for $(v^A)^{-1}$ and $(v^D)^{-1}$. These inverse functions exist because of Assumption 3(ii). Moreover, if w_- and h_- are fixed, then each of the curves $v = v^D(u, w_-)$ and $v = v^A(u, w_-)$ has a unique intersection point with the scanning curve $v = v^S(u, w_-, h_-)$, by Assumption 1(iii). We denote those points by

$$\big(u^D(w_-, h_-), v^D(w_-, h_-)\big) \quad \text{and} \quad \big(u^A(w_-, h_-), v^A(w_-, h_-)\big),$$

respectively (see Figure 5). This notation is compatible with that introduced in Section 3.

We divide the proof into two cases.

Case 1: $u_- \le u_{\rm cr}(w_-)$. In this case, we always have $v_{\rm cr} \le v_{\rm cr}(w_-)$.

(i) $v_+ \le v_-$. A Riemann solver for this case is

$$(u, v, w, h)(\xi) = \begin{cases} (u_-, v_-, w_-, h_-) & \text{if } \xi \le s = -\frac{v_+ - v_-}{u_m - u_-}, \\ (u_m, v_+, w_-, h_m) & \text{if } s < \xi \le 0, \\ (u_+, v_+, w_+, h_+) & \text{if } \xi > 0, \end{cases} \tag{53}$$

where u_m, h_m are defined by

$$(u_m, h_m) = \begin{cases} \big((v^S)^{-1}(v_+, w_-, h_-), h_-\big) & \text{if } v_+ \ge v^D(w_-, h_-), \\ \big((v^D)^{-1}(v_+, w_-), h^D((v^D)^{-1}(v_+, w_-), w_-)\big) & \text{if } v_+ < v^D(w_-, h_-). \end{cases} \tag{54}$$

In view of Figure 5, definition (54) states that if the horizontal line $v = v_+$ intersects the scanning curve $v = v^S(u, w_-, h_-)$ (i.e., if $v^+ \ge v^D(w_-, h_-)$), then u_m is the u-coordinate of

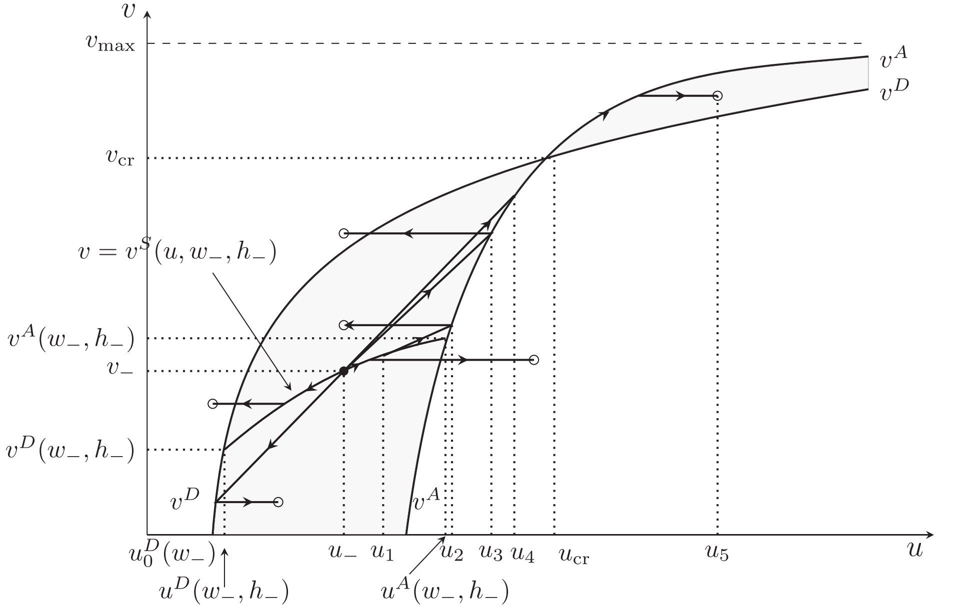

FIGURE 5 Riemann solutions in the plane (u, v) in Case 1. A full circle represents the state (u_-, w_-, h_-); various states (u_+, w_+, h_+) are represented by empty circles. The state (u_-, w_-, h_-) lies in the gray region, which is the set Ω_{w_-} in the (u, v)-plane; the states (u_+, w_+, h_+), which belong to Ω_{w_+} can well lie outside Ω_{w_-}. See Figure 8 for a representation of Ω_w for two different values of w.

the point of intersection; else (if $v^+ < v^D(w_-, h_-)$), u_m is the u-coordinate of the point of intersection of $v = v_+$ with the curve $v = v^D(u, w_-)$.

The Riemann solver (53) has the following short notation:

$$(u_-, v_-, w_-, h_-) \xrightarrow{\text{ScS or DS}} (u_m, v_+, w_-, h_m) \xrightarrow{\text{SS}} (u_+, v_+, w_+, h_+), \tag{55}$$

where arrows point to the increasing direction of ξ and x. Notice the jump in w which occurs in the last wave, which is not visible in Figure 5.

(ii) $v_+ > v_-$. In this case, the structure of the Riemann solver is

$$(u_-, v_-, w_-, h_-) \xrightarrow{\text{ScS or ScAS or ScAS+AR}} (u_m, v_+, w_-, h_m) \xrightarrow{\text{SS}} (u_+, v_+, w_+, h_+), \tag{56}$$

where

$$(u_m, h_m) = \begin{cases} \left((v^S)^{-1}(v_+, w_-, h_-), h_-\right) & \text{if } v_+ \le v^A(w_-, h_-), \\ \left((v^A)^{-1}(v_+, w_-), h^A((v^A)^{-1}(v_+, w_-), w_-)\right) & \text{if } v_+ > v^A(w_-, h_-). \end{cases} \tag{57}$$

The solution (56) drawn in the (u, v)-phase plane is in the part of Figure 5 above the line $v = v_-$. Assumption 2(v) ensures that, for every $v_- < v_+ \le v_{\max}$, the line $v = v_+$ intersects the curve $v = v^A(u, w_-)$, and hence the existence of (u_m, h_m). The first part

$$(u_-, v_-, w_-, h_-) \xrightarrow{\text{ScS or ScAS or ScAS+AR}} (u_m, v_+, w_-, h_m)$$

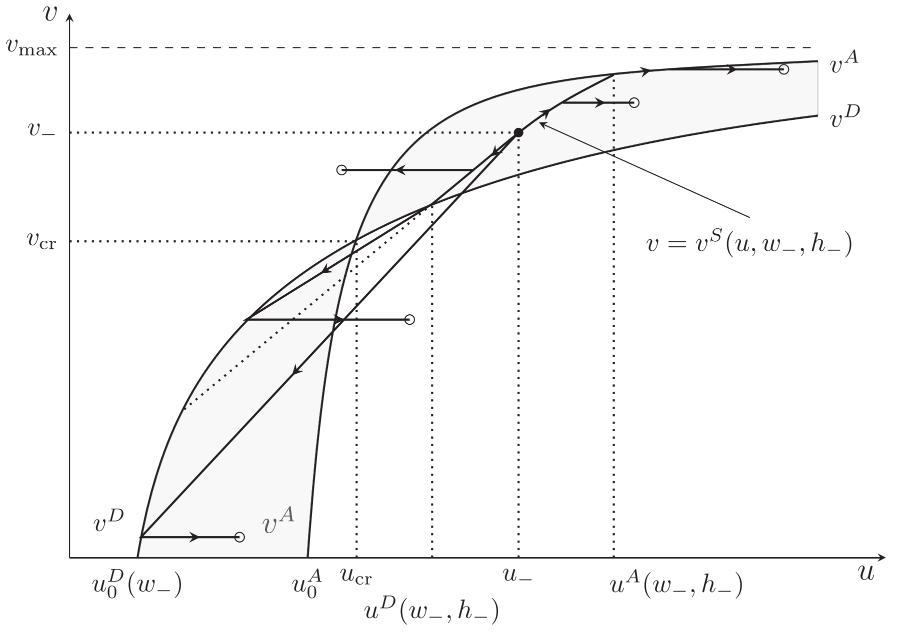

FIGURE 6 Riemann solutions in Case 2. Notations are as in Figure 5. The oblique dotted line separates the case when the first part of (58) is a scanning shock followed by a deceleration shock from the case when that part is just formed by a deceleration shock.

of the solver may consist of either a scanning shock, a scanning to acceleration shock, or else a scanning to acceleration shock followed by an acceleration rarefaction wave, in the increasing order of v. In the last case, the rarefaction wave is pasted to the preceding shock wave.

Case 2: $u_- > u_{\rm cr}(w_-)$. In this case, we always have $v_- > v_{\rm cr}(w_-)$; we refer to Figure 6.

(i) $v_+ \le v_-$. For this subcase, the Riemann solver is

$$(u_-, v_-, w_-, h_-) \xrightarrow{\text{ScS or ScS+DS or DS}} (u_m, v_+, w_-, h_m) \xrightarrow{\text{SS}} (u_+, v_+, w_+, h_+), \tag{58}$$

and (u_m, h_m) is decided by (54). This case is similar to (55) of Case 1(i), except that the single deceleration shock DS in (55) is replaced by two deceleration shocks if $v_+ < v^D(w_-, h_-)$ and

$$\frac{v_- - v_+}{u_- - u_m} < \frac{v_- - v^S\left(u^D(w_-, h_-), w_-, h_-\right)}{u_- - u^D(w_-, h_-)}.$$

(ii) $v_+ > v_-$. The Riemann solver for this subcase is depicted in the part of Figure 6 above the line $v = v_-$. Its structure is

$$(u_-, v_-, w_-, h_-) \xrightarrow{\text{ScR or ScR+AR}} (u_m, v_+, w_-, h_m) \xrightarrow{\text{SS}} (u_+, v_+, w_+, h_+), \tag{59}$$

where (u_m, h_m) is decided by (57).

This proves the existence of a solution to the Riemann problem for system (11) with initial data (52) in Ω. We now prove the uniqueness.

Any Riemann initial value (52) in Ω belongs to one of the disjoint Cases 1(i), 1(ii), 2(i), and 2(ii) listed above. For each case, there is a Riemann solver provided by (55), (56), (58), and (59), respectively. These Riemann solvers are monotone in v. Therefore, it remains to show that they are the only ones with monotone v.

Consider Case 1(i) where $u_- \leq u_{\mathrm{cr}}(w_-)$ and $v_+ \leq v_-$. The Riemann solver proved for this case is given by (55), which is a short notation for (53) and (54). If there was another Riemann solver with monotone v, then its form would be

$$(u_-, v_-, w_-, h_-) \to (u_1, v_1, w_-, h_1) \to \cdots \to (u_k, v_k, w_-, h_k) \to$$

$$\to (u_m, v_+, w_-, h_m) \xrightarrow{\text{SS}} (u_+, v_+, w_+, h_+) \tag{60}$$

with some $v_- > v_1 > \ldots > v_k > v_+$ connected by $\xrightarrow{\text{ScS or DS}}$ because there are no deceleration rarefaction waves (see Section 6).

In the Riemann solver (60), the speeds of the waves joining a state with v_j with a state with v_{j+1}, $j = 1, \ldots, k-1$, must be increasing; moreover, these speeds must be less or equal to 0. However, the hypotheses $v^A_{uu}, v^D_{uu}, v^S_{uu} < 0$, made in Assumption 3, force the speeds of these waves to decrease as j increases, leading to a contradiction.

The proofs for the other cases are similar and hence omitted. $\square$

Remark 5. As a corollary of Theorem 5, the same conclusion on the uniqueness also applies to the HLWR model in Ref. 34.

Remark 6. The Riemann solver constructed in the proof of Theorem 5 is monotone in the velocity v. Such a solver is "rational,"in the sense that it represents the behavior of a rational driver, who avoids to perform a rapid sequence of unnecessary accelerations and decelerations. The opposite behavior could be dubbed as "irrational,"since it produces waste of resources (fuel, state of the car). If we do not require the monotonicity of v, then uniqueness fails because of the large number of waves of the model (see Section 6); such nonuniqueness allows different nondeterministic driving habits. Nonuniqueness of solutions also occurs for the HLWR model [34, Section 6] as well as for related porous media models with hysteresis.[39] In the former paper, some examples of nonuniqueness are given, which still apply here, as a consequence of an "irrational" behavior; in the latter, a maximum principle for hysteresis led to discard some solutions.

Remark 7. Stationary waves may occur for fixed w, and then only u and h jump, as in the HLWR model.[34] However, in the HARZ model they may also involve a jump of w (as well as u and h, in general). This reflects the fact that the eigenvalue 0 has multiplicity two.

8 | THE EFFECTS OF HETEROGENEITY OF DRIVERS ON STOP-AND-GO WAVES

In this section, we demonstrate through examples the effects of both hysteresis and different driving behaviors on vehicular traffic flows. Moreover, we confirm the TVD property (33) for v by the numerical simulations.

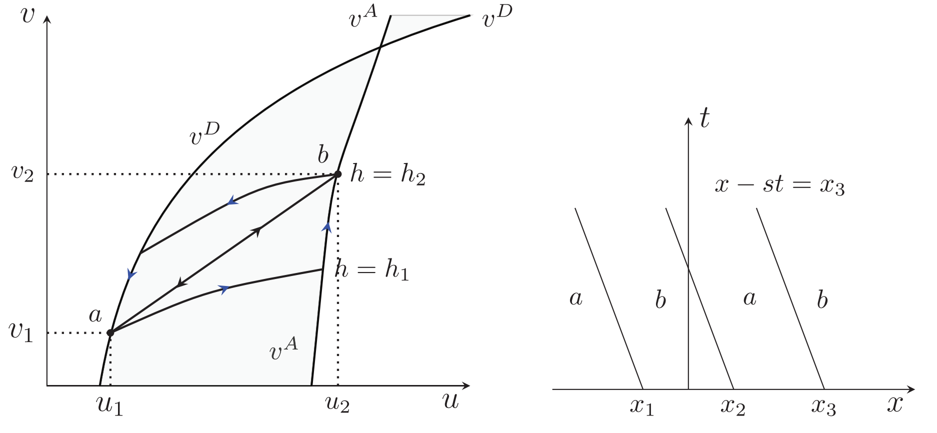

FIGURE 7 Stop-and-go solutions: left, in the (u, v)-plane; right, in the (x, t)-plane. Here, w is constant. Blue arrows indicate the loop formed by the traveling waves that approximate the shocks.

In particular, Example 1, which is essentially taken from Ref. 34, shows that the existence of a stop-and-go wave does not depend on the presence of w but on the hysteretic behavior of the model. The chord between two states p and q in the (u, v)-plane is denoted by $\mathrm{ch}(p, q)$. For two curves ϕ and ψ in the (u, v)-plane, we use the notation $\phi \prec \psi$ if ϕ lies below ψ.

Example 1 (Existence of stop-and-go waves). A stop-and-go wave has at least a pair of sharp wave fronts: one is a deceleration shock while the other is an acceleration shock. Visually, these two shock fronts often travel at the same speed, forming a slow traffic segment moving through the vehicles upstream.

Solutions with such a wave pattern can be constructed as follows. Pick two states

$$a := (u_a, h_a, w) \quad \text{and} \quad b := (u_b, h_b, w)$$

in the zone $u < u_{\mathrm{cr}}$, such that $u_a = u^D(h_a, w)$, $u_b = u^A(h_b, w)$. We refer to Figure 7 on the left. If the difference $v_b - v_a$ is large enough, then the chord-above-scanning condition (39) holds, that is, $v^S(\cdot, w_l, h_a) \prec \mathrm{ch}(a, b)$. Notice that the chord-below-scanning condition (40) is always fulfilled because of Assumption 3(ii). This condition also plays a key role in the following examples about the decay, persistence, and emergence of a stop-and-go wave, where for clarity is referred as chord-above-scanning condition.

By Theorem 2, there is a shock wave from (u_a, v_a) to (u_b, v_b) and, by Theorem 3, there is another shock wave from (u_b, v_b) to (u_a, v_a); both shock waves have the same speed $s < 0$. Stop-and-go solutions can be constructed using these two shocks. For example, consider the solution (u, v) of the inviscid system (11), shown in Figure 7 on the right. The speeds of cars at any given time t alternate as x increases, from slow (with velocity v_a) to fast (with velocity v_b). The wave pattern shape is steady because all boundaries of speed alternation travel at the same speed $s < 0$, so that the length of each speed zone does not change. Notice that the traveling waves approximating the shocks form a whole counterclockwise loop.

In Examples 2–4, we study the effect of different driving habits on the *decay* of a stop-and-go wave. We recall that by *decay* we mean the spatial decay as $x \to -\infty$, and not the usual time decay for $t \to +\infty$ considered in hyperbolic equations. The starting point is the following.

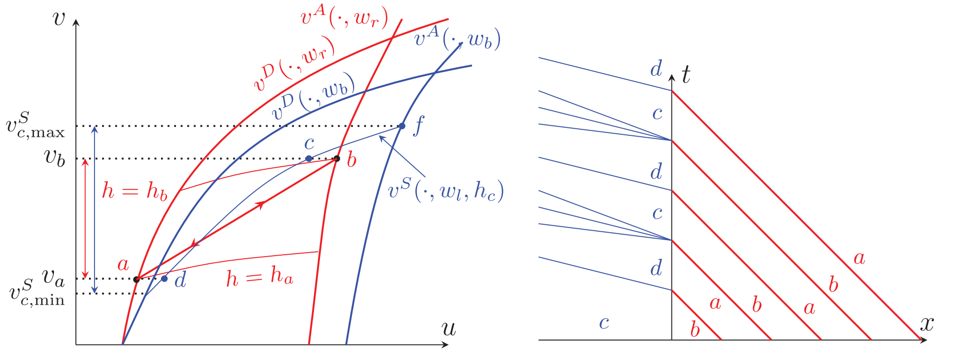

FIGURE 8 Decay of a stop-and-go wave (see Example 2). Curves and points corresponding to w_r and w_l are depicted in red and blue, respectively. Thin (thick) curves represent scanning shock and rarefaction waves (acceleration and deceleration shocks). We use the same notation in the following figures.

Suppose a vehicle platoon consists of two types of drivers: the drivers of vehicles in the $x > 0$ part of the platoon (at $t = 0$) are characterized by $w = w_r$, those of vehicles in the $x < 0$ part have $w = w_l$. We assume (see Figure 8)

$$w_l > w_r. \tag{61}$$

Assume at $t = 0$ there is a stop-and-go wave pattern in the $x > 0$ zone, while the vehicles in $x < 0$ zone are uniformly in the state c, where $v_c = v_b$. As in Example 1, in the $x > 0$ part we pick two states

$$a = (u_a, h_a, w_r) \quad \text{and} \quad b = (u_b, h_b, w_r)$$

to form a periodic stop-and-go wave pattern (see Figure 8 on the left). In the (x, t)-plane, the parallel shock waves $a \to b$ and $b \to a$ will propagate to the left to interact with the stationary shock at $x = 0$ (see Figure 8 on the right) across which w changes. After the shocks in the $x > 0$ part have interacted with the stationary shock at $x = 0$, new Riemann problems in the $x < 0$ side must be solved. The issue is the following:

Does the stop-and-go wave decay after it enters the $x < 0$ zone?

We use the following notation. For the scanning curve $v = v^S(u, w_l, h_c)$ through c, we denote

$$v^S_{c,\max} := \max_u v^S(u, w_l, h_c), \quad v^S_{c,\min} := \min_u v^S(u, w_l, h_c).$$

Example 2 (Decay of a stop-and-go wave, Part I). Assume that the curve $v = v^S(u, w_l, h_c)$ is "stiff enough,"that is, see Figure 8 on the left,

$$[v_a, v_b] \subseteq [v^S_{c,\min}, v^S_{c,\max}]. \tag{62}$$

Denote as d the unique point on the curve $v = v^S(u, w_l, h_c)$ with $v_d = v_a$. For future reference, we denote here and in the following by f the intersection of the scanning curve through d with the acceleration curve $v = v^A(u, w_l)$.

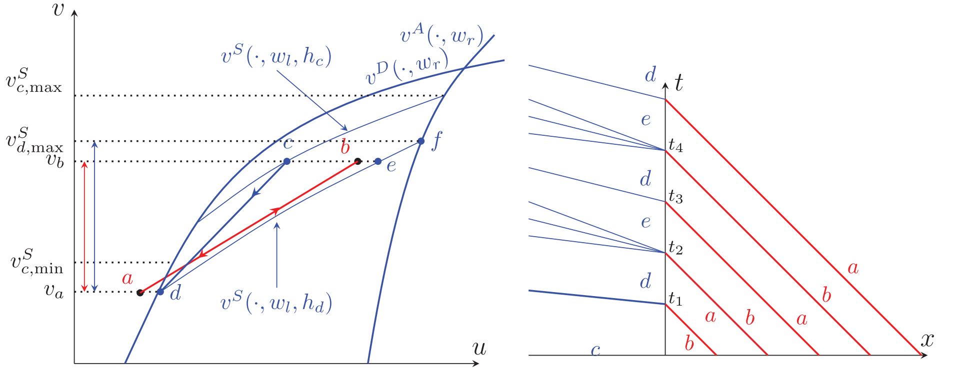

FIGURE 9 Decay of a stop-and-go wave, see Example 3, Case (i). The curves $v^A(\cdot, w_r)$ and $v^D(\cdot, w_r)$, which are as in Figure 8, are not depicted.

The jumps between states c and d are resolved by shock and rarefaction waves, alternatively, with $h = h_c$ and $w = w_l$; this reduces the HARZ model (11), in the region $x < 0$, to a scalar conservation law with strictly concave flux (see Assumption 3(ii)). These waves bounce back and forth along the same scanning curve $h = h_c$, reducing the system to the standard LWR model. Then the spatial decay of oscillations, for $x \to -\infty$, follows from the string stability of the LWR model [37, Th. 4.1].

Example 3 (Decay of a stop-and-go wave, Part II). Differently from Example 2, we now assume the scanning curve $v = v^S(\cdot, w_l, h_c)$ is "not stiff enough,"that is,

$$[v_a, v_b] \nsubseteq [v^S_{c,\min}, v^S_{c,\max}], \tag{63}$$

which implies $v^S_{c,\min} \geq v_a$. Let d be the unique state on $v = v^D(u, w_l)$ with $v = v_a$. We have two cases: either $v^S_{d,\max} \geq v_b$ or $v^S_{d,\max} < v_b$. We deal with the first case and treat the second in Example 4.

Assume $v^S_{d,\max} \geq v_b$, that is, see Figure 9,

$$[v_a, v_b] \subseteq [v_a, v^S_{d,\max}] = [v^S_{d,\min}, v^S_{d,\max}]. \tag{64}$$

By Theorem 5, since the scanning curve through c does not reach the line $v = v_a$, then at time t_1 the interaction $c \to a$ is solved as

$$c \xrightarrow{\text{ScDS}} d \xrightarrow{\text{SS}} a. \tag{65}$$

The state c is connected to d by a scanning-to-deceleration shock. At time t_2, the interaction $d \to b$ is solved as

$$d \xrightarrow{\text{ScR}} e \xrightarrow{\text{SS}} b, \tag{66}$$

where the state e is the intersection point of the scanning curve through d with the horizontal line $v = v_b$; it is connected to d by a scanning rarefaction wave. At time t_3, the interaction $e \to a$

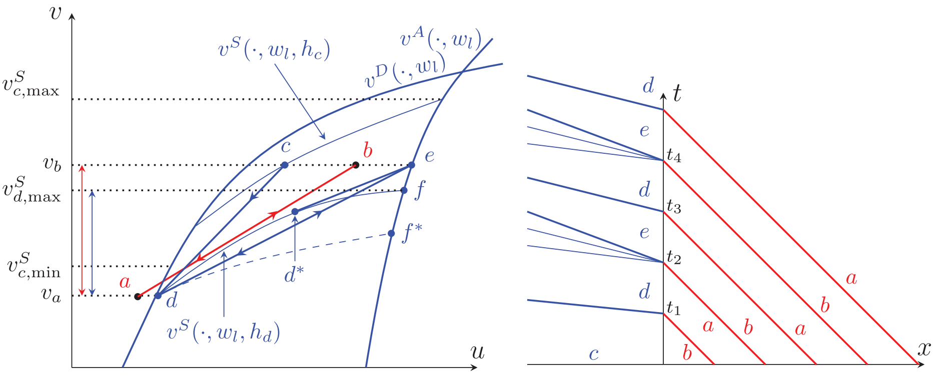

FIGURE 10 Persistence of a stop-and-go wave, see Example 4, Case (i). The single thick blue lines on the right represent deceleration shocks; the other thick lines are acceleration shocks.

is solved as

$$e \xrightarrow{\text{ScS}} d \xrightarrow{\text{SS}} a. \tag{67}$$

At last, at time t_4 the interaction $d \to b$ is solved as in (66), and so on. As a consequence, we deduce the following.

(i) Assume $v^S(\cdot, w_l, h_d) \prec \text{ch}(c, d)$. Then the leading deceleration shock $c \to d$ does not interact with the scanning waves in $x < 0$ region originated at $x = 0^-$; this is also true for the waves produced by the interactions of the scanning waves, because they lie on the same scanning curve (because of the monotonicity in v of the Riemann solver, see Theorem 5). In this case, the waves issued from point $x = 0$ after time $t = t_2$ interact just as in Example 2, leading to the spatial decay of these waves.

(ii) Assume $v^S(\cdot, w_l, h_d) \nprec \text{ch}(c, d)$. Then, the curve $v^S(\cdot, w_l, h_d)$ intersects the chord $\text{ch}(c, d)$ and so the shock $c \to d$ interacts with the scanning wave $d \xrightarrow{\text{ScR}} e$ originated at point $(x, t) = (0, t_2)$. This interaction will replace the velocity v_d on the right of the shock $c \to d$, a local minimum for v, by a higher one, reducing the oscillations of v even more than in case (i). This is confirmed by numerical computations in the next example (see Figure 11).

The conclusion is that if (63) and (64) hold, then the stop-and-go wave decays when it enters the $x < 0$ region. Notice that in both cases of this example we have $v^S(\cdot, w_l, h_d) \succ \text{ch}(d, e)$, because of the concavity of the scanning curves.

Example 4 (The condition for decay). We continue the analysis of Example 3 by assuming (63) and $v^S_{d,\max} < v_b$, that is, $[v_a, v_b] \nsubseteq [v_a, v^S_{d,\max}]$ (see Figure 10).

At time t_1, the interaction $c \to a$ is solved as in (65). Let e denote the intersection point of the acceleration curve $v = v^A(\cdot, w_l)$ with the horizontal line $v = v_b$.

(i) Assume $v^S(\cdot, w_l, h_d) \nprec \text{ch}(d, e)$, so that the chord $\text{ch}(d, e)$ is partially under the scanning curve $v^S(\cdot, w_l, h_d)$. Then, the interaction $d \to b$ is solved by

$$d \xrightarrow{\text{ScR}} d^* \xrightarrow{\text{ScAS}} e \xrightarrow{\text{SS}} b, \tag{68}$$

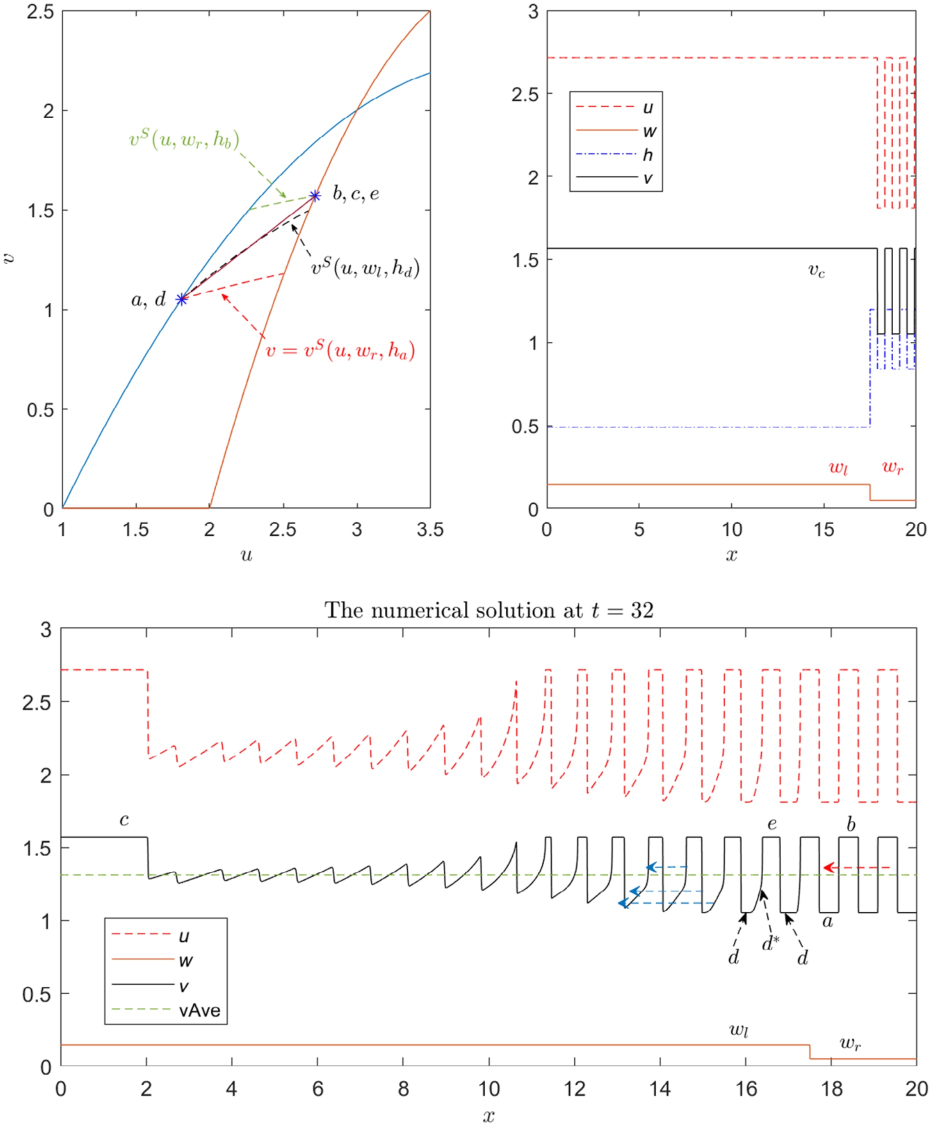

FIGURE 11 See Example 4(i); w is discontinuous at point $x = 17$. Above: initial data in the (u, v)- and $(x, \cdot)$-planes. Below: the numerical solution at time $t = 32$.

where d^* is the point on the curve $v^S(\cdot, w_l, h_d)$, whose tangent line at d^* goes through e. Due to their wave speed difference, the shocks and the waves $d \to d^* \to e$ will interact with the other shocks $e \to d$. Such interactions squeeze out the extremes of v between them, and hence reduce the amplitudes of the oscillations of the velocity.

This is also illustrated by the numerical computations shown in Figure 11. This one and the following numerical simulations have been obtained with an upwind scheme inspired by the one used for the HLWR model in Ref. 34. We refer to Appendix A for more details.

In that figure, the fundamental diagram is set such that the functions v^A and v^D do not depend on w, while the function $v^S(\cdot, w, h)$ does. This setup forces states a and d (b and e) to coincide in the (u, v)-plane. The stop-and-go wave oscillating between a and b is present in the right region, where $w = w_r$. It persists in the left region, because the chord $\mathrm{ch}(d, e)$ (which coincides with $\mathrm{ch}(a, b)$) is above the scanning curve $v^S(\cdot, w_l, h_d)$. As a reference, we also drew the average velocity $v_{\mathrm{Ave}} := (v_a T_a + v_b T_b)/(T_a + T_b)$, where T_a and T_b are the time intervals where the periodic solution in the right part stays in state a or b, respectively.

Therefore, when the condition $v^S(\cdot, w_l, h_d) \prec \mathrm{ch}(d, e)$ fails, then the amplitude of the oscillations of the velocity shrinks. If this condition still holds as the solution evolves, then such a decay of oscillations continues until the oscillations disappear. Else, such decay stops. We discuss this issue in Remark 8.

(ii) Assume $v^S(\cdot, w_l, h_d) \prec \mathrm{ch}(d, e)$. Then, the interaction $d \to b$ is resolved by

$$d \xrightarrow{\text{ScAS}} e \xrightarrow{\text{SS}} b. \tag{69}$$

The waves $d \to e$ emanating from points $(x, t) = (0, t_2)$ or $(0, t_4)$ in Figure 10 on the right are actually shocks parallel to the shock $e \to d$. Together, these parallel shocks $d \to e$ and $e \to d$ form a stop-and-go wave in the $x < 0$ region. In this case, the stop-and-go wave in the $x > 0$ region persists after it enters the $x < 0$ region, albeit the wave speeds may change.

The analysis of the previous examples shows that the propagation of a stop-and-go wave into a zone with larger w is dictated by the mutual position of the curve $v^S(\cdot, w_l, h_d)$ and the chord $\mathrm{ch}(d, e)$. Indeed, notice that in Example 2 the points c and e coincide. In particular, the stop-and-go wave persists if $v^S(\cdot, w_l, h_d) \prec \mathrm{ch}(d, e)$; for brevity, we call *chord-above-scanning* such a condition.

In Examples 2–4 we showed that “stiff” scanning curves can depress velocity oscillations while “flat” scanning curves let stop-and-go waves persist. In the following example, we show that “flat” scanning curves can produce, as a consequence of different driving habits, a stop-and-go wave from oscillations that otherwise would decay.

Example 5 (Speed oscillations sharpen up to stop-and-go waves if the chord-above-scanning condition holds). In this example, we reverse the values of w_l and w_r used in the last examples, while keeping the initial oscillations of v as they were there; hence

$$w_l < w_r. \tag{70}$$

In this case, we have $v^S(\cdot, w_l, h_d) \prec \mathrm{ch}(d, e)$; on the contrary, the chord-above-scanning condition fails on the right. More precisely, the initial data in the right part consist of alternating constant pieces of states a and b, which lie on the same scanning curve (see Figure 12); vehicles on the left part are uniformly in state c, which is assumed to coincide with a in the (u, v)-plane. In Figure 12, we assume, for simplicity, $v^D(\cdot, w_r) = v^D(\cdot, w_l)$ and $v^A(\cdot, w_r) = v^A(\cdot, w_l)$ as in Figure 11; moreover, we take $w_l = 1/20$ and $w_r = 1/5$.

After a sufficiently large time, the waves in the right part would interact and *decrease* the speed oscillations if w does not change. But, before that can happen, the waves enter the left region and then they sharpen up to a *persistent stop-and-go wave*, as in Examples 2–4; this is due to the chord-under-scanning condition. This is illustrated in Figure 12.

The results of the previous examples are resumed in Table 1.

Remark 8. We showed in Example 4(i) that the condition $v^S(\cdot, w_l, h_d) \not\prec \mathrm{ch}(d, e)$ leads to the decay of the stop-and-go wave; the issue is *how long* this decay lasts. The interactions of the waves in the

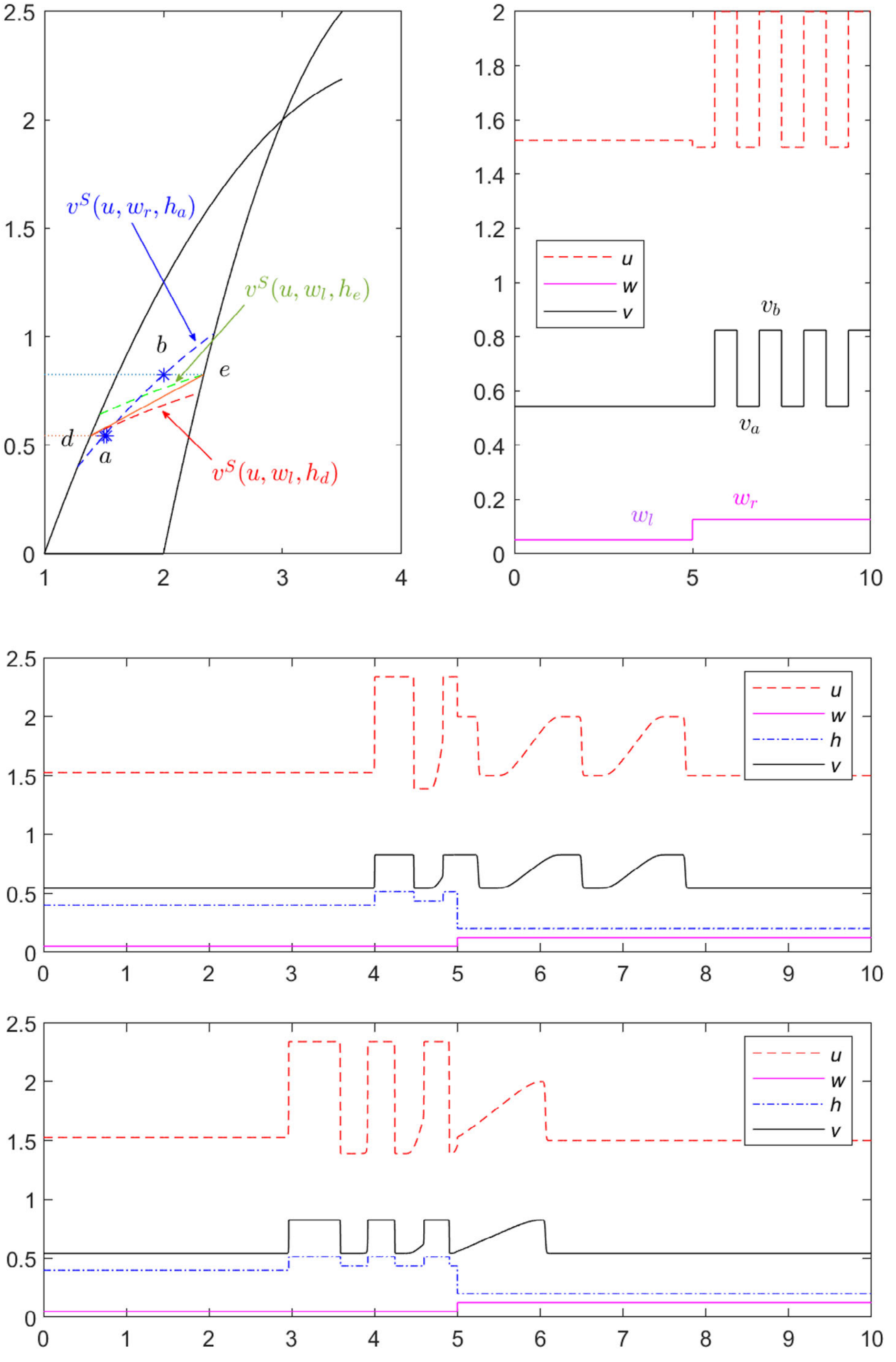

FIGURE 12 See Example 5; here w is discontinuous at point $x = 5$. Above: the initial data in the (u, v)- and $(x, \cdot)$-planes. Center and below: the solution at times $t = 4$ and $t = 7$, respectively.

TABLE 1 Overview of the positions of the scanning curves and the corresponding chords, and the results for the stop-and-go wave.

Example	Condition	Stop-and-go wave
1	$v^S(\cdot, w_l, h_a) \prec \mathrm{ch}(a, b)$	persists
2	$v^S(\cdot, w_l, h_d) \succ \mathrm{ch}(d, e)$	decays
3	$v^S(\cdot, w_l, h_d) \succ \mathrm{ch}(d, e)$	decays
4(i)	$v^S(\cdot, w_l, h_d) \not\prec \mathrm{ch}(d, e)$	decays
4(ii)	$v^S(\cdot, w_l, h_d) \prec \mathrm{ch}(d, e)$	persists
5	$v^S(\cdot, w_l, h_d) \prec \mathrm{ch}(d, e)$	emerges and persists

$x < 0$ region yield new states; we denote by $d(x)$ and $e(x)$ the states, at the position x, such that

$$v_{d(x)} = \inf_{t > x/\sigma} v(x,t), \quad v_{e(x)} = \sup_{t > x/\sigma} v(x,t),$$

where $\sigma < 0$ is the speed of the deceleration shock $c \to d$ and $v(x,t)$ is the velocity at (x,t) in the interaction. Then, we have $d(0^-) = d$ and $e(0^-) = e$, where d and e are the states in Example 4 and either $v(0^-,t) = v\left(u(0^-,t), w_l, h_d\right)$ or $v(0^-,t) = v\left(u(0^-,t), w_l, h_e\right)$. In the previous examples, we had

$$v_{d(x)} = \inf_{t > x/\sigma} v^S(u(x,t), w_l, h_d), \quad v_{e(x)} = \sup_{t > x/\sigma} v^S(u(x,t), w_l, h_e),$$

because d and e lay on $v^D(\cdot, w_l)$ and $v^A(\cdot, w_l)$, respectively.

From above, the function $d(x)$ increases as $x \to -\infty$ while $e(x)$ decreases. As a consequence, as far as the condition

$$v^S(u(x,t), w_l, h_d(x)) \not\prec \mathrm{ch}\left(d(x), e(x)\right) \tag{71}$$

is fulfilled, then the stop-and-go wave decays. Otherwise, the decay stops at the point where (71) is no more fulfilled.

Remark 9. It is believed in Ref. 27 that the formation of stop-and-go waves is due to the presence of both timid and aggressive drivers. The previous examples show that this is not always the case, and that the presence of stop-and-go waves depends on the "chord-above-scanning" condition.

Our next example concerns the decay of speed oscillations due to negative hysteresis.

Example 6 (Faster decay of speed oscillations under negative hysteresis). The previous Examples 1–5 show that in the congested zone, where positive (i.e., counterclockwise) hysteresis loops occur, the model (11) supports *persistent* stop-and-go waves. We may guess that in the free zone, where hysteresis loops become negative (i.e., clockwise), the model should yield a *decay* of speed oscillations, as is the case in real-world traffic flows.

On the other hand, the previous examples also show that in the congested zone the decay of speed oscillations seems strictly related to the failure of the "chord-above-scanning" condition: in such a case, the decay is caused by the interaction of shock and rarefaction waves of the same characteristic family.

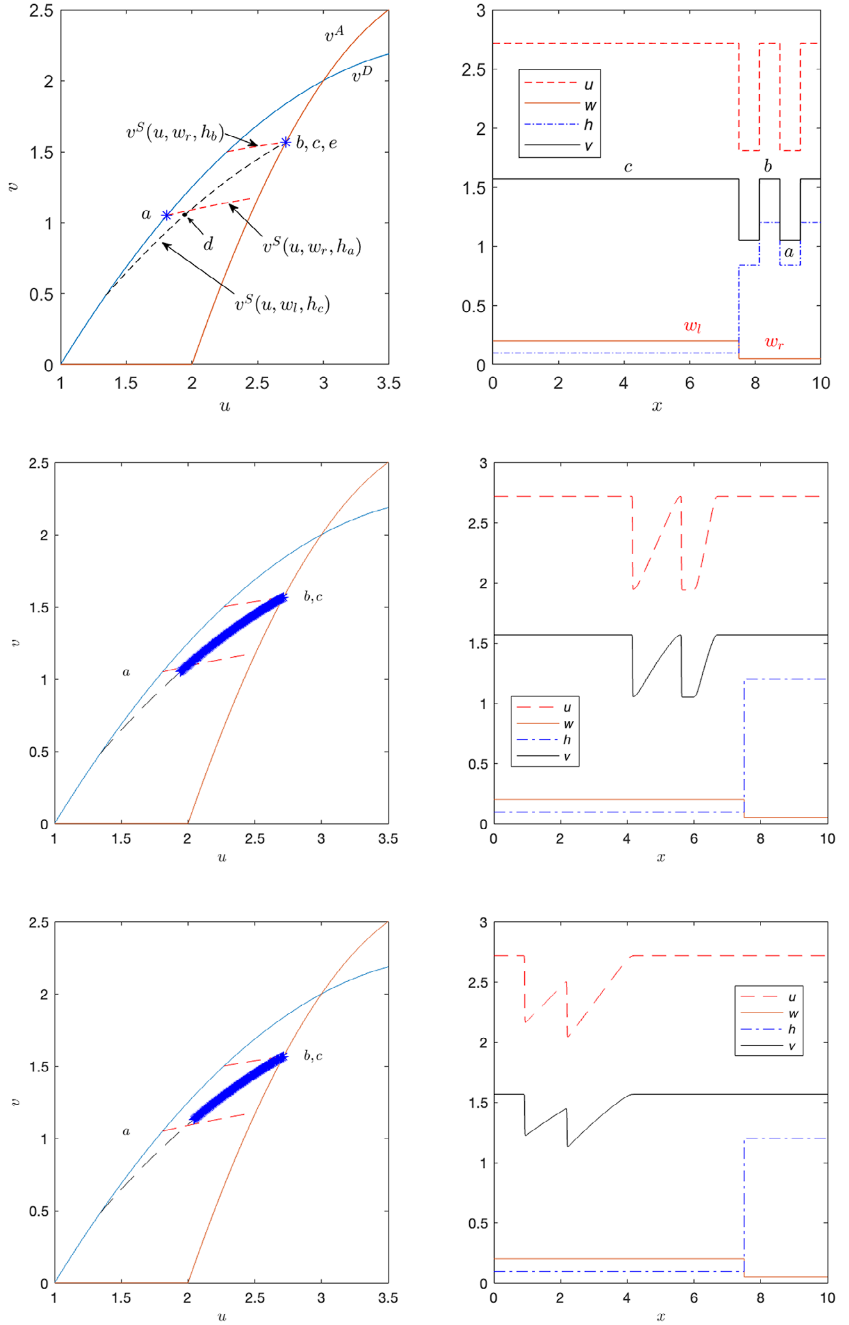

FIGURE 13 See Example 6(i); here w is discontinuous at $x = 7.5$. Above: initial data in the (u, v)- and $(x, \cdot)$-planes. Center and below: the solution at $t = 5$ and $t = 10$, respectively.

It is then natural to investigate which of these two mechanisms damp speed oscillations harder. To answer this question, we compute the numerical solutions of system (11) for two initial data.

(i) The first initial data are given in Figure 13; we assume, for simplicity, that v^A and v^D do not depend on w, as in Figure 11. Then in the plane (u, v) the states b, c, d coincide, but not a and

d. In the right part of the platoon, we have $w_r = 1/20$. The scanning curve through a and b is "flat" enough to allow a stop-and-go wave connection (see Example 1). In the left part, drivers are in the state c, which coincides with b in the (u, v)-plane, and $w_l = 1/5$. Both flows in the right and left side take place in the congested zone.

In this case, the scanning curve through e is "stiff" enough to make the chord-above-scanning condition fail. Then, according to Example 2, the speed oscillations over the right part of the platoon decay after they propagate into the left side.

The thick blue curve is formed by asterisks, which show the values of the solution in the left side: they lie on the scanning curve through e. See the center-right and below-right panels in Figure 13.

(ii) The second initial data (see Figure 14) keep in the right side of the platoon the same initial data of case (i). The only difference from (i) is that the state c now has $w_l = 1$, for which the hysteresis there is *negative*. Then, the flow is congested on the right of the platoon and free on the left.

The numerical solution for these initial data is shown in Figure 14. It is clear that, in this case, the speed oscillations in Figure 14 are much less than those in Figure 13.

This suggests that negative hysteresis can suppress speed oscillations *harder* than what the genuine nonlinearity of a scalar conservation law can do.

For some speed ranges, drivers of a platoon of cars are usually a mixture of positive hysteresis type, indicated by $w = w_r$ part of top-left in Figure 14, and negative hysteresis type, the $w = w_l$ part. We have seen in Example 5 that positive hysteresis loops with chord-above-scanning condition can sharpen speed oscillations into stop-and-go waves, while negative hysteresis dampens such oscillations (see Example 6). Example 6 shows that if a segment of a traffic flow with negative hysteretic drivers is sufficiently longer than the stop-and-go wave length, then the speed oscillations will be dampened enough so that the chord-above-scanning condition fails when these oscillations propagate into the subsequent segment with positive hysteresis drivers. Then the speed oscillation will continue the decay, as indicated by Example 4. Else, if the chord-above-scanning condition still holds as these oscillations propagate into a segment of positive hysteresis drivers, then the oscillations will sharpen up to a stop-and-go wave again.

As a further development of Example 6, we now consider a numerical example where positive and negative hysteresis drivers are finely mixed in a vehicle platoon, and investigate the effect of such a mixture on the decay of stop-and-go waves. We notice that the paper[23] shows that a high ratio of positive to negative drivers is associated to the *growth* of oscillations. Below, we show that a low ratio is associated to *decay*.

Example 7 (Effect of mixture of drivers of positive and negative hysteresis). The right side is shown as the interval $19 < x < 20$ of the initial value and boundary value is $w_r = 1.7/20 =: w_0$. The velocity v oscillates at $x = 20$ between 1.2 and 1.5 to form a stop-and-go wave propagating over the interval $19 < x < 20$ towards the left (see Figure 15).

The period of oscillation at the boundary $x = 20$ is $t = 2$. On the left of $x = 19$, the parameters w of drivers are $w_0 = 1.7/20$ and $w_1 = 1$, mixed periodically at the ratio of $2 : 1$; this means each grid point with $w = w_1 = 1$ is followed by two grid points with $w = w_0$. The values of u and h corresponding $w = w_1$ grid points are chosen so that $v_1 = v^A(u_1, w_1) = 1.5$. This setup simulates stop-and-go waves propagating into a platoon whose drivers are a mixture of positive hysteresis $w = w_0$ and negative hysteresis $w = w_1$ types. The segment $19 < x < 20$ is to confirm that $w = w_0$ does support the stop-and-go wave as seen in $19 < x < 20$ part of Figure 15. Figure 15 shows the

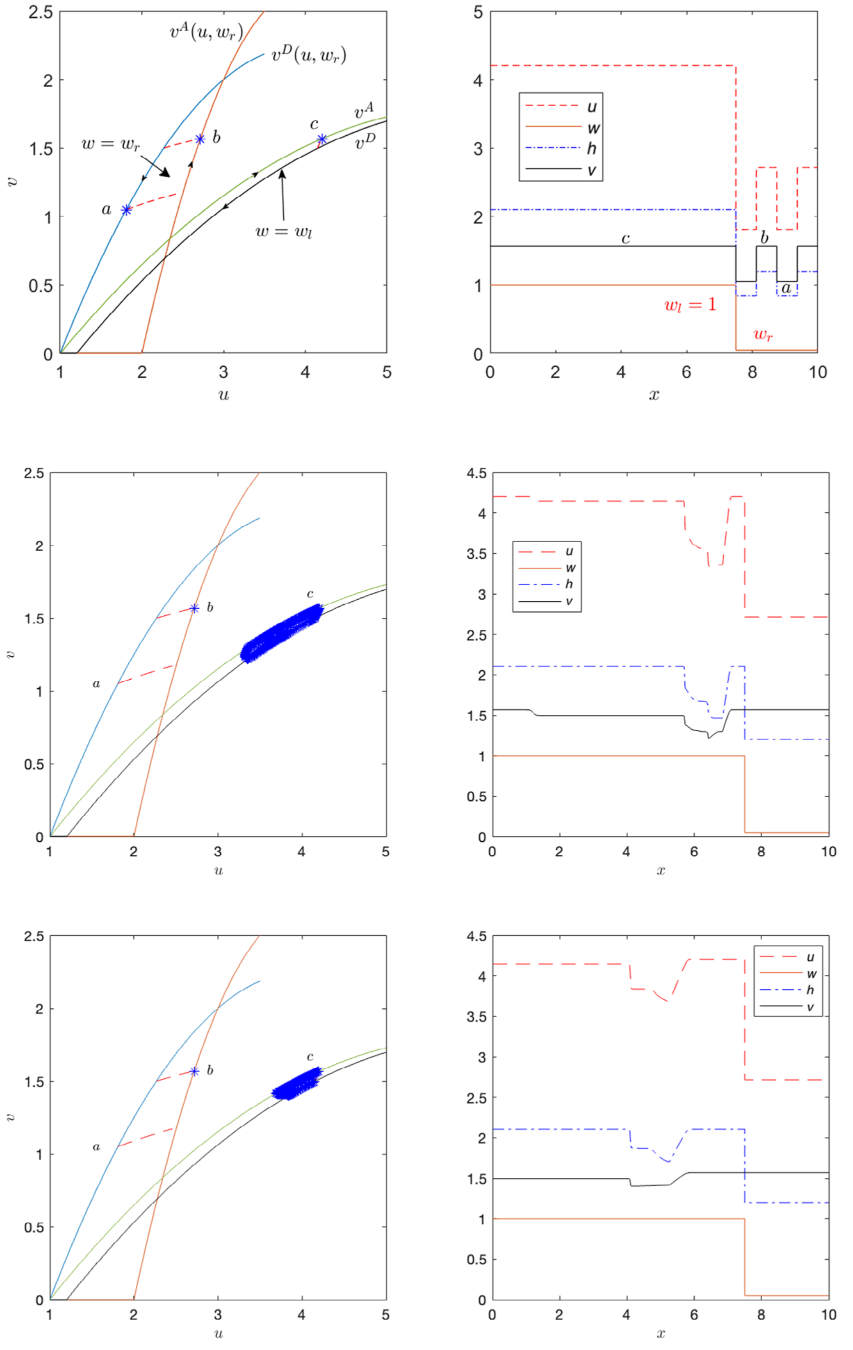

FIGURE 14 See Example 6(ii); here w is discontinuous at $x = 7.5$. Above: initial data in the (u, v)- and $(x, \cdot)$-planes. Center and below: the solution at $t = 5$ and $t = 10$, respectively.

numerical solution of $v(x, t = 60.625)$ and demonstrates that the oscillations of $v(x, t)$ decay as they propagates to the left. If the ratio of w_0 versus w_1 drivers is $3 : 1$, then the stop-and-go wave does not decay. But, reducing the period of oscillation at the boundary $x = 20$ from $t = 2$ to 0.5, the stop-and-go wave decays again. Typically, higher-frequency speed oscillations decay faster.

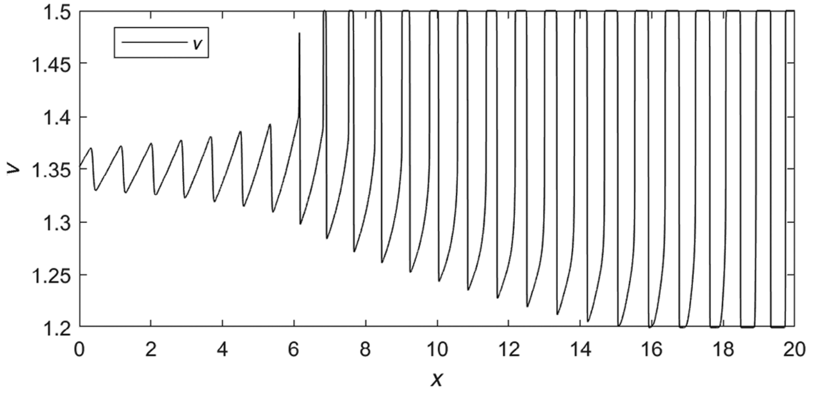

FIGURE 15 Numerical solution of $v(x, t)$ at $t = 60.625$. The stop-and-go wave over $x > 19$, where the hysteresis is positive, propagates into the $x < 19$ part of the platoon where drivers of both positive and negative hysteresis types are well mixed. Speed oscillations decay as they propagate toward the left.

Remark 10. In some recent papers, see, for instance, Ref. 23 clockwise (negative) loops were observed in "*congested* traffic flows."While this phenomenon cannot be modeled by the HLWR system, on the contrary the HARZ model can (see Examples 6(ii) and 7). The reason is the inhomogeneity of the drivers, which makes v_{cr} depend on w.

9 | CONCLUSIONS

In this paper, we embedded a hysteretic behavior into the famous ARZ model for traffic flows; we called HARZ such a model. Without hysteresis, the ARZ model cannot model stop-and-go waves; on the contrary, under the presence of hysteresis, such waves appear. Therefore, stop-and-go waves are a result of hysteresis. The HARZ model has another advantage, namely, it enables to study the effects of different driving habits on stop-and-go waves.

First, we performed a rigorous analysis of the properties of the HARZ model: existence and uniqueness of a Riemann solver, existence of viscous profiles for the discontinuous waves, and existence of a maximum principle for the diffusive HARZ model.

Second, we focused on several case studies to test the model. We showed that the HARZ model is perfectly capable of describing stop-and-go waves. The decay or persistence of such waves is characterized by a simple geometric "chord-above-scanning" condition. Positive hysteresis loops satisfying such condition support stop-and-go waves. Both negative hysteresis loops and the failure of the chord-above-scanning condition dampen stop-and-go waves.

ACKNOWLEDGMENTS

A.C. is a member of the *Gruppo Nazionale per l'Analisi Matematica, la Probabilità e le loro Applicazioni* (GNAMPA) of the *Istituto Nazionale di Alta Matematica* (INdAM) and acknowledges financial support from this institution through the INdAM - GNAMPA Project, codice CUP E53C23001670001. He also acknowledges financial support from the PRIN 2022 project *Modeling, Control and Games through Partial Differential Equations* (D53D23005620006), funded by the European Union - Next Generation EU.

Open access publishing facilitated by Universita degli Studi di Ferrara, as part of the Wiley - CRUI-CARE agreement.

DATA AVAILABILITY STATEMENT

Data sharing is not applicable to this article as no new data were created or analyzed in this study.

ORCID

Andrea Corli https://orcid.org/0000-0003-0600-4208

REFERENCES

1. Lighthill MJ, Whitham GB. On kinematic waves. II. A theory of traffic flow on long crowded roads. *Proc R Soc Lond Ser A*. 1955;229:317-345.
2. Richards PI. Shock waves on the highway. *Oper Res*. 1956;4:42-51.
3. Aw A, Rascle M. Resurrection of "second order" models of traffic flow. *SIAM J Appl Math*. 2000;60(3):916-938.
4. Zhang HM. A non-equilibrium traffic model devoid of gas-like behavior. *Transp Res B*. 2002;36:275-290.
5. Payne HJ. Models of Freeway Traffic and Control. In: Bekey, GA, ed., *Mathematical Models of Public Systems*. Vol. 1. Simulation Council, La Jolla; 1971:51-61.
6. Whitham GB. *Linear and Nonlinear Waves*. Pure and Applied Mathematics. Wiley-Interscience; 1974.
7. Goatin P. The Aw-Rascle vehicular traffic flow model with phase transitions. *Math Comput Model*. 2006;44(3-4):287-303.
8. Colombo RM. Hyperbolic phase transitions in traffic flow. *SIAM J Appl Math*. 2002;63(2):708-721.
9. Garavello M, Goatin P. The Aw-Rascle traffic model with locally constrained flow. *J Math Anal Appl*. 2011;378(2):634-648.
10. Garavello M, Piccoli B. Traffic flow on a road network using the Aw-Rascle model. *Commun Partial Differ Equ*. 2006;31(1-3):243-275.
11. Herty M, Rascle M. Coupling conditions for a class of second-order models for traffic flow. *SIAM J Math Anal*. 2006;38(2):595-616.
12. Godvik M, Hanche-Olsen H. Existence of solutions for the Aw-Rascle traffic flow model with vacuum. *J Hyperbolic Differ Equ*. 2008;5(1):45-63.
13. Chen T, Jiang W, Li T. On the stability of the improved Aw-Rascle-Zhang model with Chaplygin pressure. *Nonlinear Anal Real World Appl*. 2021;62:Paper No. 103351.
14. Greenberg JM. Extensions and amplifications of a traffic model of Aw and Rascle. *SIAM J Appl Math*. 2001;62(3):729–745.
15. Lebacque J, Mammar S, Schnetzler B, Haj-Salem H. Generic second order traffic flow modeling. In: *Transportation and Traffic Theory 2007*. Elsevier; 2007:755-776.
16. Andreianov B, Sylla A. Existence analysis and numerical approximation for a second-order model of traffic with orderliness marker. *Math Models Methods Appl Sci*. 2022;32(7):1295-1348.
17. Garavello M, Han K, Piccoli B. *Models for Vehicular Traffic on Networks*. American Institute of Mathematical Sciences (AIMS); 2016.
18. Garavello M, Piccoli B. *Traffic Flow on Networks*. AIMS Series on Applied Mathematics. Vol 1. American Institute of Mathematical Sciences (AIMS); 2006.
19. Ahn S, Vadlamani S, Laval J. A method to account for non-steady state conditions in measuring traffic hysteresis. *Transp Res B*. 2013;34:138-147.
20. Andreotti E, Bazzani A, Rambaldi S, Guglielmi N, Freguglia P. Modeling traffic fluctuations and congestion on a road network. *Adv Complex Syst*. 2015;18(3-4):1550009.
21. Blank M. Hysteresis phenomenon in deterministic traffic flows. *J Stat Phys*. 2005;120:627-658.
22. Blank M. Travelling with/against the flow. Deterministic diffusive driven systems. *J Stat Phys*. 2008;133:773-796.
23. Chen D, Laval JA, Ahn S, Zheng Z. Microscopic traffic hysteresis in traffic oscillations: a behavioral perspective. *Transp Res B*. 2012;46:1440-1453.
24. Chowdhury D, Santen L, Schadschneider A. Statistical physics of vehicular traffic and some related systems. *Phys Rep*. 2000;329(4-6):199-329.
25. Deng H, Zhang H. On traffic relaxation, anticipation, and hysteresis. *Transp Res Rec*. 2015;2491:90-97.
26. Laval JA. Hysteresis in traffic flow revisited: an improved measurement method. *Transp Res B*. 2011;45:385-391.
27. Laval JA, Leclercq L. A mechanism to describe the formation and propagation of stop-and-go waves in congested freeway traffic. *Philos Trans R Soc A*. 2010;368:4519-4541.

28. Treiterer J, Myers J. The hysteresis phenomenon in traffic flow. In: Buckley DJ, ed. *Proceedings of the Sixth Symposium on Transportation and Traffic Theory*. Vol 6. 1974:13-38.
29. Yeo H, Skabardonis A. Understanding stop-and-go traffic in view of asymmetric traffic theory. In: Lam W, Wong S, Lo H, eds. *Transportation and Traffic Theory 2009: Golden Jubilee*. Springer; 2009:99-115.
30. Zhang HM. A mathematical theory of traffic hysteresis. *Transp Res B*. 1999;33:1-23.
31. Newell GF. Theories of instability in dense highway traffic. *Oper Res Soc Jpn*. 1962;5:9-54.
32. Newell GF. Instability in dense highway traffic, a review. In: Almond J, ed. *Proceedings of Second Symposium on the Theory of Road Traffic Flow*. Organisation for Economic Co-operation and Development; 1965:73–83.
33. Yeo H. *Asymmetric Microscopic Driving Behavior Theory*. Ph.D. Thesis, University of California Transportation Center, University of California, Berkeley; 2008.
34. Corli A, Fan H. Hysteresis and stop-and-go waves in traffic flows. *Math Models Methods Appl Sci*. 2019;29(14):2637-2678.
35. Edie LC, Bavarez E. Generation and propagation of stop-start traffic waves. In: Edie LC, Herman R, Roghery R, eds. *Vehicular Traffic Science*. Elsevier; 1967:26-37.
36. Fan H. Conservation laws with hysteretic fluxes. *J Differ Equ*. 2024;394:1-30.
37. Corli A, Fan H. String stability in traffic flows. *Appl Math Comput*. 2023;443:Paper No. 127775.
38. Dafermos CM. *Hyperbolic Conservation Laws in Continuum Physics*. 4th ed. Springer-Verlag; 2016.
39. Corli A, Fan H. Two-phase flow in porous media with hysteresis. *J Differ Equ*. 2018;265(4):1156-1190.
40. Fan H, Shu C-W. Existence and computation of solutions of a model of traffic involving hysteresis. *SIAM J Appl Math*. 2020;80(6):2319-2337.
41. Fan H, Shu C-W. High order numerical methods for flows with hysteretic fluxes. *Appl Numer Math*. 2023;184:234-252.

How to cite this article: Corli A, Fan H. The hysteretic Aw–Rascle–Zhang model. *Stud Appl Math*. 2024;e12769. https://doi.org/10.1111/sapm.12769

APPENDIX A: TECHNICAL DETAILS

For all numerical experiments in this paper, we used the first-order upwinding scheme proposed in Refs. 34, 40. The constitutive functions used in the computation are given by Ref. 41 as follows.

For $0 < w < 1/4$:

$$\begin{cases} v^D(u) = \frac{1}{4}\left[9-(u-4)^2\right], & 1 \le u \le 3, \\ v^A(u) = \frac{2}{3}\left[4-(u-4)^2\right], & 2 \le u \le 3, \\ v^S(u,w,h) = w\left[9-(u-4)^2\right]+h, & 0 \le h \le 2-8w, \\ h^D(u,w) = \left(\frac{1}{4}-w\right)\left[9-(u-4)^2\right], & \\ u^D(h,w) = 4-\sqrt{9-\frac{h}{1/4-w}}, & \\ h^A(u,w) = \frac{8}{3}-9w+\left(w-\frac{2}{3}\right)(u-4)^2, & \\ u^A(h,w) = 4-\sqrt{\frac{8/3-9w-h}{2/3-w}}. & \end{cases}$$

For $w \geq 1/4$:

$$\begin{cases} v^A(u,w) = \dfrac{9}{5} - \dfrac{9}{125}(u-6)^2 & \text{if } 1 \leq u \leq 6 \text{ and } 0 \text{ if } u \in [0,1), \\ v^D(u,w) = \dfrac{9}{5} - \dfrac{9}{125}(u-6.2)^2 & \text{if } 1.2 \leq u \leq 6 \text{ and } 0 \text{ if } u \in [0,1.2), \\ v^S(u,w,h) = 4 - \dfrac{4}{25}(u-6-h)^2, & \\ h^D(u,w) = u - 6 + \dfrac{5}{\sqrt{20}}\sqrt{11 + 9(u-6.2)^2/25}, & \\ u^D(h,w) = 6.2 + \dfrac{25}{22}\left(\dfrac{8(h-0.2)}{5} - \sqrt{\dfrac{144(h-0.2)^2}{125} + \dfrac{484}{25}}\right), & \\ h^A(u,w) = u - 6 + \dfrac{5}{\sqrt{20}}\sqrt{11 + 9(u-6)^2/25}, & \\ u^A(h,w) = 6 + \dfrac{25}{22}\left(\dfrac{8h}{5} - \sqrt{\dfrac{144h^2}{125} + \dfrac{484}{25}}\right). & \end{cases}$$